Article

The neural mechanisms supporting the rise and fall of maternal aggression

https://doi.org/10.1038/s41586-026-10354-5

Received: 4 January 2025

Accepted: 3 March 2026

Published online: 15 April 2026

Open access

Check for updates

Takashi Yamaguchi[1,9]✉, Rongzhen Yan[1,9], Mashrur Khan[1], Sota Kuno[2], Kanishk Tewatia[1], Takuya Osakada[1], Srinivas Parthasarathy[3,4,5], Michael E. Pacold[2], Nirao M. Shah[3,4,6] & Dayu Lin[1,7,8]✉

Maternal aggression enables lactating females to protect their vulnerable young[1,2], yet its rapid emergence after birth and swift decline when pups are absent remain poorly understood. Our study reveals the critical role of the pathway from posterior amygdala cells expressing oestrogen receptor alpha (PA^{Esr1}) to the ventrolateral part of ventromedial hypothalamus cells expressing neuropeptide Y receptor 2 ($VMHvl^{Npy2r}$) in the rise and fall of maternal aggression. Projection-specific manipulations and recordings show that PA^{Esr1} cells projecting to the VMHvl are naturally active during attack and are required for maternal aggression. During lactation, PA-to-$VMHvl^{Npy2r}$ synapses potentiate and $VMHvl^{Npy2r}$ cell excitability increases, enabling heightened aggression. PA^{Esr1} neurons express abundant oxytocin receptors, allowing oxytocin to boost PA output; after pup removal, declining oxytocin levels reduce PA drive and dampen maternal aggression, a deficit restored by pup reunion or optogenetic elevation of oxytocin. These findings reveal multiple forms of plasticity in a defined PA^{Esr1}–$VMHvl^{Npy2r}$ circuit that collectively implement the adaptive, need-based control of maternal aggression.

After birth, young mammals are vulnerable and require protection. To ensure offspring survival, mothers of many species vigorously attack intruders, a behaviour that is known as maternal aggression[1,2]. As its name implies, maternal aggression is largely confined to the maternal period. In mice and rats, non-lactating females rarely attack conspecific intruders; aggression rises sharply 1 day after parturition, peaks during the first postpartum week, then gradually declines and disappears by the end of lactation[3–5]. This pronounced behavioural transition is thought to reflect changes in aggression circuitry, and—given its autonomous nature—pregnancy- and lactation-associated hormones have long been considered key contributors[6].

In the late 1970s, it was shown that oestrogen and progesterone regimens mimicking pregnancy, together with nipple development and pup suckling, could induce aggression in virgin female mice, whereas sex hormones alone were ineffective[6,7]. Preventing pup suckling through thelectomy (nipple removal) similarly blocked maternal aggression in mouse mothers[8]. These findings indicate that pregnancy-related hormonal changes, combined with postpartum nursing, are required to initiate maternal aggression. However, how female aggression circuits are reorganized during pregnancy and how pup suckling promotes maternal aggression remain unclear nearly five decades later.

Esr1-expressing cells in the VMHvl ($VMHvl^{Esr1}$) are essential for both male aggression and female aggression[9–12]. In female mice, $VMHvl^{Esr1}$ cells comprise two functionally and anatomically distinct subpopulations: medially biased *Npy2r*-expressing cells ($VMHvl^{Npy2r}$) are essential for female aggression[13], whereas laterally biased cholecystokinin A receptor (encoded by *Cckar*) cells ($VMHvl^{Cckar}$ cells), which are largely *Npy2r*-negative but *Esr1*-positive ($VMHvl^{Npy2r(-)Esr1(+)}$), mediate female sexual receptivity[13–15]. During lactation, $VMHvl^{Npy2r}$ cells, but not $VMHvl^{Npy2r(-)Esr1(+)}$ or $VMHvl^{Cckar}$ cells, exhibit elevated in vivo responses to intruders compared with virgin female mice[13,15], although the cellular or synaptic mechanisms underlying this enhancement remain unclear.

Beyond the VMHvl, the female aggression circuit is largely uncharacterized. We previously found that PA^{Esr1} cells, which are predominantly glutamatergic, provide strong excitatory input to the VMHvl and drive male aggression[16]. Inhibiting PA^{Esr1} cells projecting to the VMHvl ($PA^{Esr1\rightarrow VMHvl}$) impairs male aggression, whereas activating them promotes attack[16,17]. Moreover, the PA^{Esr1}–VMHvl pathway is plastic: repeated victories potentiate PA^{Esr1}-to-VMHvl connections and ultimately enhance aggression[18,19].

Given the critical role of the PA^{Esr1}–VMHvl pathway in male aggression and experience-dependent plasticity, we examined whether this circuit also contributes to maternal aggression and whether circuit plasticity supports the marked escalation of aggression during lactation. We found that the PA^{Esr1}–VMHvl circuit is essential for maternal aggression, but operates through mechanisms distinct from those in male mice. Specifically, oxytocin-dependent modulation enables rapid, need-based adjustment of maternal aggression to protect offspring.

Maternal aggression needs $PA^{Esr1\rightarrow VMHvl}$ cells

To determine whether $PA^{Esr1\rightarrow VMHvl}$ cells are necessary for maternal aggression, we virally expressed hM4Di in $PA^{Esr1\rightarrow VMHvl}$ cells by injecting a retrograde HSV expressing Cre-dependent *Flpo* into the VMHvl

[1]Institute of Translational Neuroscience, New York University Langone Medical Center, New York, NY, USA. [2]Department of Radiation Oncology, New York University Langone Health, New York, NY, USA. [3]Departments of Psychiatry and Behavioral Sciences, Stanford University, Stanford, CA, USA. [4]Department of Neurobiology, Stanford University, Stanford, CA, USA. [5]Accent Therapeutics, Lexington, MA, USA. [6]Department of Obstetrics and Gynecology, Stanford University, Stanford, CA, USA. [7]Department of Psychiatry, New York University Langone Medical Center, New York, NY, USA. [8]Department of Neuroscience, New York University Langone Medical Center, New York, NY, USA. [9]These authors contributed equally: Takashi Yamaguchi, Rongzhen Yan. ✉e-mail: Takashi.Yamaguchi@nyulangone.org; Dayu.Lin@nyulangone.org

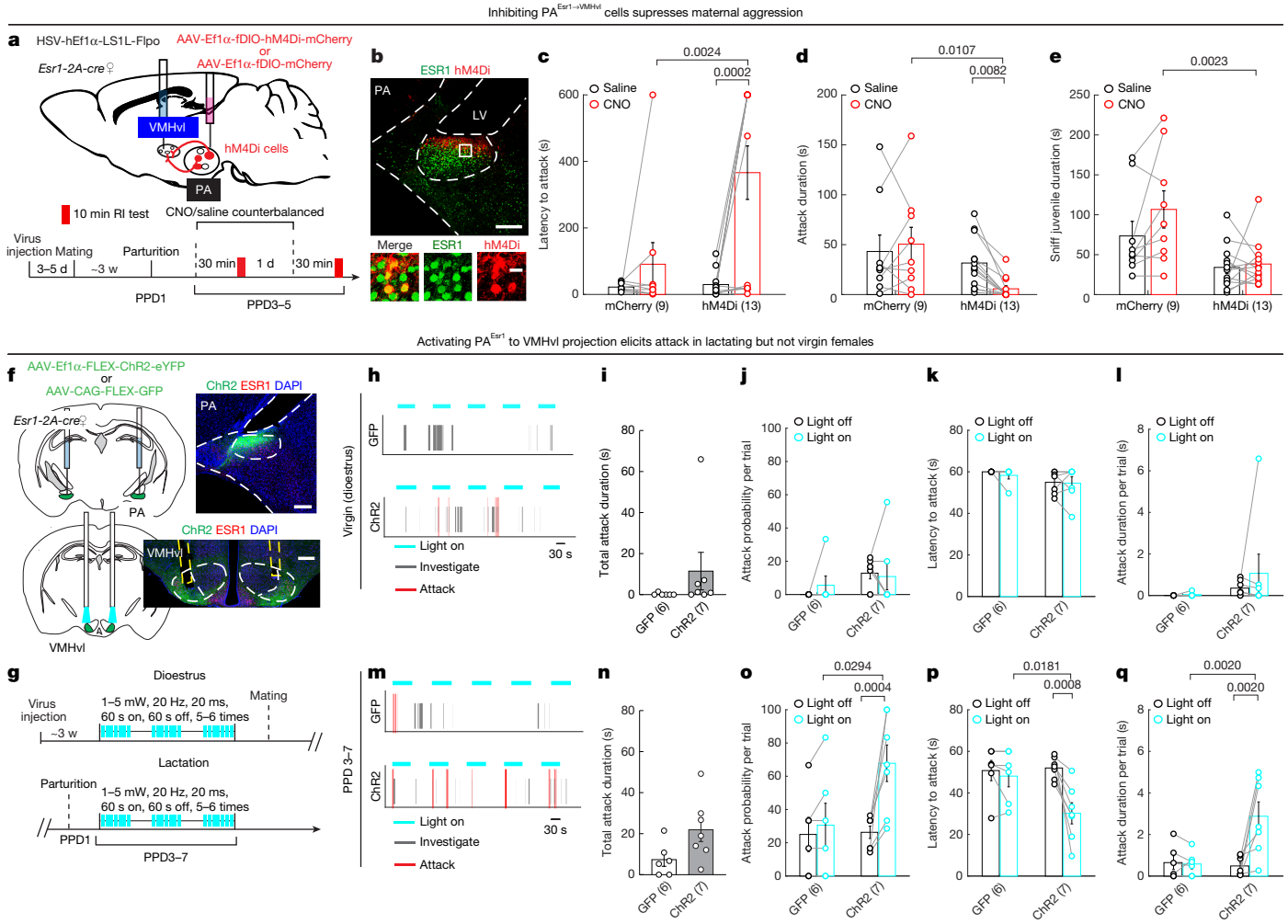

Fig. 1 | The PA^{Esr1}–VMHvl pathway bidirectionally modulates maternal aggression. a, Experimental schematics and test schedule. **b**, Histological images showing hM4Di expression and ESR1 staining in the PA. Bottom, magnified views of the areas indicated by boxes. **c**,**d**, Attack latency increased (**c**) and attack duration decreased (**d**) after CNO injection in hM4Di mice, but not mCherry mice. For mice showing no attack, the latency was set to 600 s. **e**, The juvenile investigation duration was unchanged after CNO or saline injections. **f**, Experimental schematic and representative images showing ChR2–eYFP (green) and ESR1 (red) expression in the PA and VMHvl. Blue, DAPI. Brain illustrations were adapted from the Allen Brain Reference Atlas (https://atlas.brain-map.org). **g**, Experimental timeline. **h**,**m**, Behaviours toward juvenile intruders with or without light stimulation in virgin (**h**) and lactating (**m**) female mice. **i**,**n**, The total attack duration of ChR2 and GFP virgin (**i**) and lactating (**n**) female mice. **j**–**l**, There was no change in attack probability (**j**), latency to attack from light onset (**k**) or attack duration per trial (**l**) during the light-on versus light-off periods in both ChR2 and GFP virgin female mice. **o**–**q**, In lactating ChR2 mice, but not GFP mice, the attack probability increased (**o**), the latency to attack decreased (**p**) and the average attack duration per trial increased (**q**). Data are mean ± s.e.m. The numbers in parentheses represent the number of animals. Statistical significance was determined using mixed-effects analysis with repeated measures followed by Bonferroni's multiple-comparison test (**c**–**e**,**j**–**l** and **o**–**q**), Mann–Whitney *U*-tests (**i**) and unpaired *t*-tests (**n**). All *P* values <0.05 are indicated. All tests were two-tailed. Detailed statistics are provided in Supplementary Table 1. Scale bars, 200 μm (**b** (top) and **f**) and 20 μm (**b** (bottom)).

and AAV-Ef1α-fDIO-hM4Di–mCherry (control: mCherry) into the PA of virgin C57BL/6N (C57) *Esr1-2A-cre* × Swiss–Webster (SW) F_1 hybrid female mice (Fig. 1a). We used C57 × SW F_1 mice because they display more robust and reliable maternal aggression compared with C57 mice, while maintaining genetic uniformity (Supplementary Note 1). Histological analysis confirmed that the vast majority of hM4Di–mCherry-expressing cells in the PA were ESR1 positive (96.81 ± 0.03%, $n = 3$ mice; Fig. 1b). hM4Di–mCherry-positive cells comprised around 10% of all PA cells (Extended Data Fig. 1c), similar to the percentage of PA cells that express *Esr1* and retrogradely labelled with the retrograde tracer, cholera toxin B subunit (CTB), injected into the VMHvl, suggesting that most VMHvl-projecting PA^{Esr1} cells were likely targeted (Extended Data Fig. 1a–c).

After virus injection, each female was paired with a male until visibly pregnant. Maternal aggression was then assessed between postpartum day 3 (PPD3) and PPD5, 30 min after intraperitoneal (i.p.) injection of saline or clozapine *N*-oxide (CNO) on separate, counterbalanced days (Fig. 1a). After saline injection, all of the female mice attacked the juveniles rapidly and repeatedly (Fig. 1c,d). By contrast, after CNO injection, all hM4Di female mice significantly decreased attacks during the 10-min test, whereas all of the mCherry controls remained highly aggressive (Fig. 1c,d). The decreased aggression was not due to reduced social interest, as investigation duration was unaffected by PA$^{Esr1→VMHvl}$ cell inactivation. (Fig. 1e). In a separate experiment, inhibiting PA^{Esr1} cells broadly also significantly reduced maternal aggression (Extended Data Fig. 2a–d). By contrast, maternal care was unaffected by inhibition of either PA$^{Esr1→VMHvl}$ or total PA^{Esr1} populations in mothers (Extended Data Fig. 2e,m,n).

As VMHvl is also critical for female sexual behaviours[20], we also examined whether PA$^{Esr1→VMHvl}$ cells are necessary for female sexual

receptivity, assessed by rejection probability and lordosis[15,21]. Female sexual receptivity did not differ between saline- and CNO-treated days (Extended Data Fig. 2o,p). Male mice achieved intromission with comparable latencies and durations under both conditions (Extended Data Fig. 2q–u). Inhibiting PA^{Esr1} cells yielded similar results, indicating their dispensable role in female sexual behaviours (Extended Data Fig. 2f–l). Thus, $PA^{Esr1\rightarrow VMHvl}$ cells are specifically required for maternal aggression, but not other female social behaviours.

PA^{Esr1}–VMHvl drives maternal aggression

To test whether the $PA^{Esr1\rightarrow VMHvl}$ projection is sufficient to drive attack, we bilaterally injected AAV-Ef1α-FLEX-ChR2-eYFP into the PA and implanted optic fibres above the VMHvl in C57 *Esr1-2A-cre* × SW F_1 hybrid female mice (Fig. 1f). Then, 3 weeks later, we first tested stimulation-induced behaviours in dioestrous virgin females by delivering light pulses (470 nm, 20 Hz, 20 ms, 1.0–5.0 mW) for 60 s every 2–3 min after introducing a juvenile intruder (Fig. 1g). None of the dioestrous females showed time-locked attacks during PA^{Esr1}-to-VMHvl activation, although ChR2 animals attacked more than GFP animals overall during the test session (Fig. 1h–l). After the aggression test, the female mice were placed into the home cage of a sexually experienced male mouse; light stimulation did not increase female sexual receptivity (Extended Data Fig. 3a,b). Both GFP and ChR2 female mice consistently rejected male mice regardless of stimulation, and intromission never occurred (Extended Data Fig. 3b–d).

Afterwards, the test females were paired with males and terminal stimulation-evoked attack was re-examined during PPD3–PPD7, when maternal aggression is naturally expressed. After light stimulation, ChR2 animals, but not GFP animals, had a significantly increased probability of attacking the juvenile intruder (Fig. 1m–q). Light-on trials were associated with a reduced attack latency and an increased attack duration compared with the light-off trials (Fig. 1p,q). Together, these results indicate that PA^{Esr1} cells provide a critical excitatory input to the VMHvl for driving female aggression, with greater efficacy during lactation than in the virgin state.

$VMHvl^{Npy2r}$ plasticity during lactation

To address why PA inputs to the VMHvl elicit time-locked attacks in mothers but not in virgin females, we investigated VMHvl cell responses to PA inputs using in vitro patch-clamp recordings (Fig. 2a). We focused on $VMHvl^{Npy2r}$ cells given their established role in maternal aggression[13]. Indeed, direct optogenetic activation of $VMHvl^{Npy2r}$ cells reliably induced attacks in virgin females, suggesting their deterministic role in initiating female aggression (Extended Data Fig. 4). We next performed current-clamp recordings of $VMHvl^{Npy2r}$ cells and compared their spiking probability during PA-VMHvl terminal stimulation in virgin versus lactating females (PPD3–PPD5) (Fig. 2b). While PA terminal activation (1 ms, 20 Hz, 473 nm light pulses) induced action potentials in less than 15% of $VMHvl^{Npy2r}$ cells in virgin dioestrous or oestrous female mice, nearly half (11 out of 23) spiked in lactating females (Fig. 2b,c). This enhanced spiking could reflect changes in synaptic strength or intrinsic excitability.

To examine the former, we performed voltage-clamp recordings of $VMHvl^{Npy2r}$ cells in virgins and mothers (PPD3–PPD5) while optogenetically activating PA terminals to evoke excitatory postsynaptic currents (oEPSCs) and inhibitory postsynaptic currents (oIPSCs) (Fig. 2d,e). As in male mice[16], the oEPSC latency was short (mean ± s.e.m., 3.49 ± 0.38 ms), indicating a monosynaptic connection (Fig. 2f), whereas the oIPSC latency was longer (mean ± s.e.m., 12.47 ± 1.31 ms), consistent with a polysynaptic connection (Fig. 2f). During dioestrus, 65% (13 out of 20) of cells exhibited oEPSCs, whereas only 12% (2 out of 16) did so during oestrus (Fig. 2e). The oEPSC amplitude was also reduced in oestrous female mice compared with in dioestrous and lactating female mice (Fig. 2g). This difference is unlikely presynaptic, as paired-pulse ratios were comparable across reproductive states (Fig. 2h,i). The probability of evoking oIPSCs showed a similar reproductive-state dependence, consistent with their secondary nature (Fig. 2e,g). Moreover, for spontaneous excitatory postsynaptic currents (sEPSCs), but not for spontaneous inhibitory postsynaptic currents (sIPSCs), the frequency of $VMHvl^{Npy2r}$ cells was the lowest during oestrus (Fig. 2j–n). Together, these findings indicate that PA–$VMHvl^{Npy2r}$ connectivity is strongest during lactation and weakest during oestrus.

Next, we examined the intrinsic properties of $VMHvl^{Npy2r}$ cells using current-clamp recordings. Although rheobase, resting membrane potential (RMP) and input resistance did not differ across reproductive states, $VMHvl^{Npy2r}$ cells in lactating females fired more spikes across current steps and reached a higher maximal firing rate compared with in dioestrous females (Fig. 2o–t). $VMHvl^{Npy2r}$ cells in oestrous females exhibited intermediate excitability (Fig. 2o–q). Collectively, these results suggest that enhanced PA-driven spiking of $VMHvl^{Npy2r}$ cells during lactation arises from both strengthened synaptic input and increased intrinsic excitability.

The increased $VMHvl^{Npy2r}$ cell responses are also evident in vivo. As previously reported[13], Ca^{2+} responses of $VMHvl^{Npy2r}$ cells to juvenile intruders increased significantly during lactation (Extended Data Fig. 5). In lactating female mice, the peak Ca^{2+} response of $VMHvl^{Npy2r}$ cells during intruder introduction was around threefold of that in virgin females (Extended Data Fig. 5c,d,g). During social investigation, $VMHvl^{Npy2r}$ cell activity also consistently increased, although the response magnitude did not differ between virgin and lactating females (Extended Data Fig. 5e,g). Females reliably attacked the intruder only during lactation (Extended Data Fig. 5b). During attack, $VMHvl^{Npy2r}$ cells exhibited reliable, moderate activity increases (Extended Data Fig. 5f,g). Between dioestrus and oestrus, $VMHvl^{Npy2r}$ cell Ca^{2+} responses to intruders were comparable, consistent with low aggression in virgin female mice regardless of oestrous stage[11] (Extended Data Fig. 5b-g).

Limited PA-to-$VMHvl^{Npy2r(-)Esr1(+)}$ input

PA^{Esr1} cells send dense fibres to both aggression-related VMHvlm and mating-related VMHvll (Extended Data Fig. 6a,b). However, we observed no sexual behaviour change after either inhibiting $PA^{Esr1\rightarrow VMHvl}$ cells or activating PA^{Esr1}-to-VMHvl projection (Extended Data Figs. 2p–u and 3). To understand this dissociation, we investigated the connection from PA to $VMHvl^{Npy2r(-)Esr1(+)}$ cells, a population known to bidirectionally control female sexual receptivity[13,15]. Specifically, we injected AAV-hSyn-Coff/Fon-mCherry into the VMHvl of *Npy2r-ires-cre* × *Esr1-2A-Flpo* mice to label $VMHvl^{Npy2r(-)Esr1(+)}$ cells and AAV-hSyn-Chronos-GFP into the PA to enable optogenetic control of PA-to-VMHvl terminals in brain slices (Extended Data Fig. 6c). Histological analysis confirmed that the vast majority of mCherry-expressing cells were *Npy2r* negative and *Esr1* positive (94.9 ± 1.6% cells from 3 animals; Extended Data Fig. 6c,d). Notably, none of the 18 recorded $VMHvl^{Npy2r(-)Esr1(+)}$ cells in oestrous females fired a single spike after PA terminal stimulation, and only 3 out of 15 (20%) cells showed light-evoked EPSCs despite strong Chronos expression in the PA (Extended Data Fig. 6e–h,j,k,m–o). We focused on oestrous females because PA input would be most likely to influence mating-related VMHvl output during oestrus, when these cells are maximally excitable[15]. Consistent with this, PA input exerted even less influence in sexually inactive lactating females, with only 3 out of 26 (12%) $VMHvl^{Npy2r(-)Esr1(+)}$ cells showing light-evoked EPSCs (Extended Data Fig. 6k,m–o). This contrasts sharply with the 79% of aggression-related $VMHvl^{Npy2r}$ cells that exhibited oEPSCs during PA terminal stimulation in lactating females (Fig. 2e). Accordingly, $VMHvl^{Npy2r(-)Esr1(+)}$ cells exhibited lower spontaneous sEPSC frequencies during both oestrus and lactation compared with $VMHvl^{Npy2r}$ cells (Fig. 2k,m and Extended Data Fig. 6i,l,p,q).

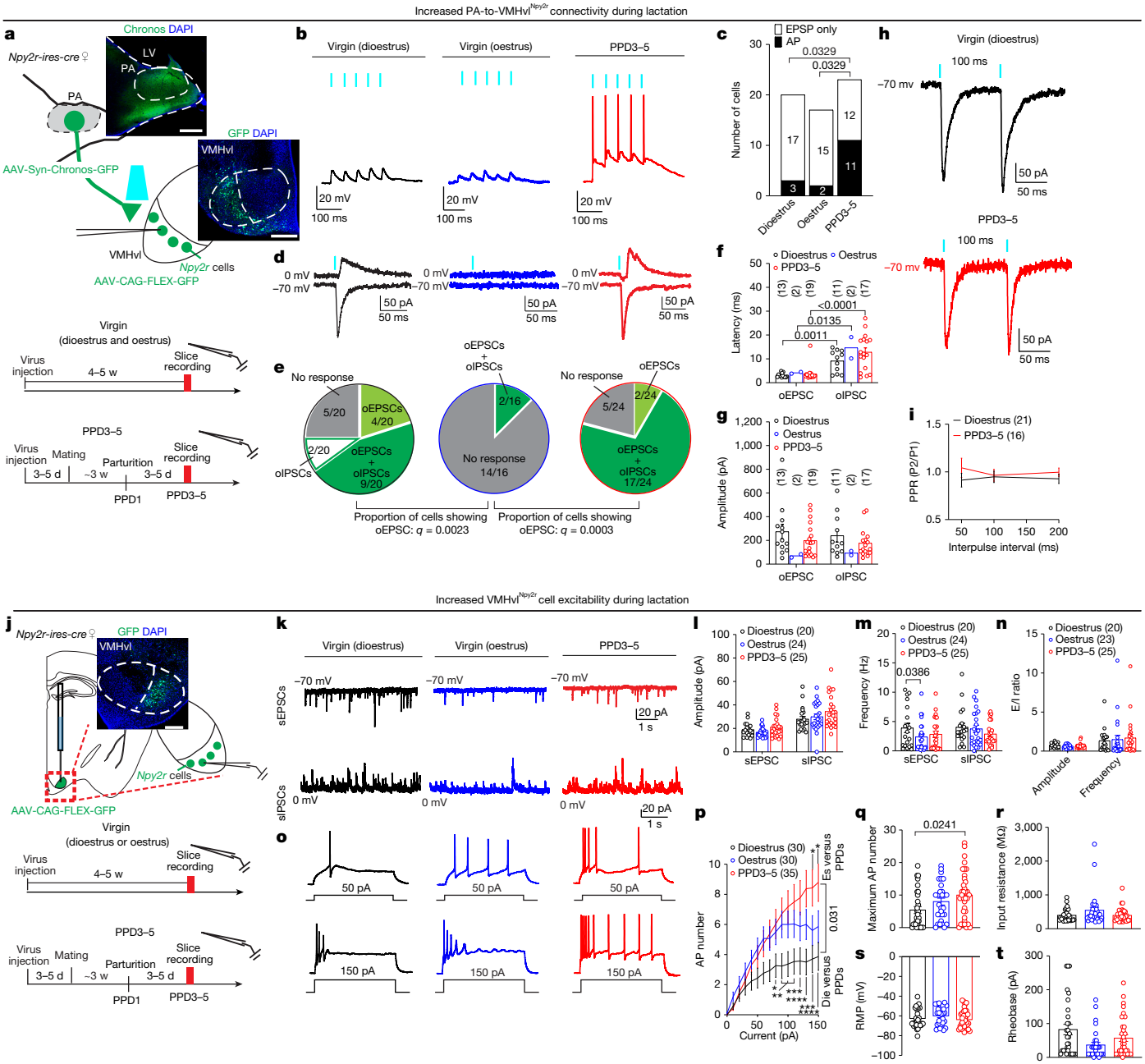

Fig. 2 | Changes in VMHvl^{Npy2r} responses to intruders and physiology properties in lactating females. a, Experimental schematic, histology and test timeline. **b**, Representative oEPSP and action potential (AP) traces evoked by 1-ms light pulses (cyan) in dioestrous (black), oestrous (blue) and lactating (red) female mice. **c**, The percentage of VMHvl^{Npy2r} cells exhibiting light-induced spiking. **d**, Example oEPSC and oIPSC traces evoked by 1-ms light pulses. **e**, The distribution of light-evoked synaptic response types. **f**,**g**, The latency (**f**) and amplitude (**g**) of oEPSCs and oIPSCs. **h**, Representative paired oEPSCs evoked at 100-ms intervals in dioestrous and lactating female mice. **i**, Paired-pulse ratios (PPRs). **j**, Experimental schematic, test schedule and representative histology for VMHvl^{Npy2r} cell recordings. Brain illustrations were adapted from the Allen Brain Reference Atlas (https://atlas.brain-map.org). **k**, Example spontaneous EPSC (sEPSC) and IPSC (sIPSC) traces across reproductive states. **l**–**n**, The sEPSC and sIPSC amplitude (**l**) and frequency (**m**) and the excitatory/inhibitory ratio (**n**). **o**, Representative current-clamp responses to 50 and 150 pA injections. **p**–**t**, *F*–*I* curves (**p**), the maximum number of APs (**q**), input resistance (**r**), RMP (**s**) and rheobase (**t**) of VMHvl^{Npy2r} cells. Data are mean ± s.e.m. The numbers in parentheses denote recorded cells. Statistical analysis was performed using Fisher's exact tests or χ^2 tests with Benjamini–Hochberg FDR correction (**c**), χ^2 tests with FDR correction (**e**), mixed-effects analysis with Bonferroni correction (**f**, **g** and **p**), two-way repeated-measures ANOVA with Bonferroni correction (**i**) and Kruskal–Wallis test with Dunn's multiple-comparison correction (**l**–**n** and **q**–**t**). Cells in **c** and **e**–**g** were from 5 dioestrous, 3 oestrous and 6 lactating female mice; in **i**, from 5 dioestrous and 6 lactating female mice; and in **l**–**n** and **p**–**t**, from 5 dioestrous, 4 oestrous and 6 lactating female mice. All *P* and *q* values <0.05 are indicated except for in **p**; $^*P < 0.05$, $^{**}P < 0.01$, $^{***}P < 0.001$, $^{****}P < 0.001$. All tests were two-tailed. Detailed statistics are provided in Supplementary Table 1. Scale bars, 200 µm (**a** and **j**).

These results suggest that, first, PA input preferentially targets VMHvl^{Npy2r} cells over VMHvl$^{Npy2r(-)Esr1(+)}$ cells, especially during lactation; second, PA inputs could not drive VMHvl$^{Npy2r(-)Esr1(+)}$ cells to spike even during oestrus, likely explaining the lack of female sexual behaviour change during PA$^{Esr1\rightarrow VMHvl}$ manipulation.

Higher PA$^{Esr1\rightarrow VMHvl}$ response in mothers

We next examined whether PA cells themselves show heightened responses to aggression-related cues during lactation, thereby contributing to elevated maternal aggression. We recorded PA$^{Esr1\rightarrow VMHvl}$ cell

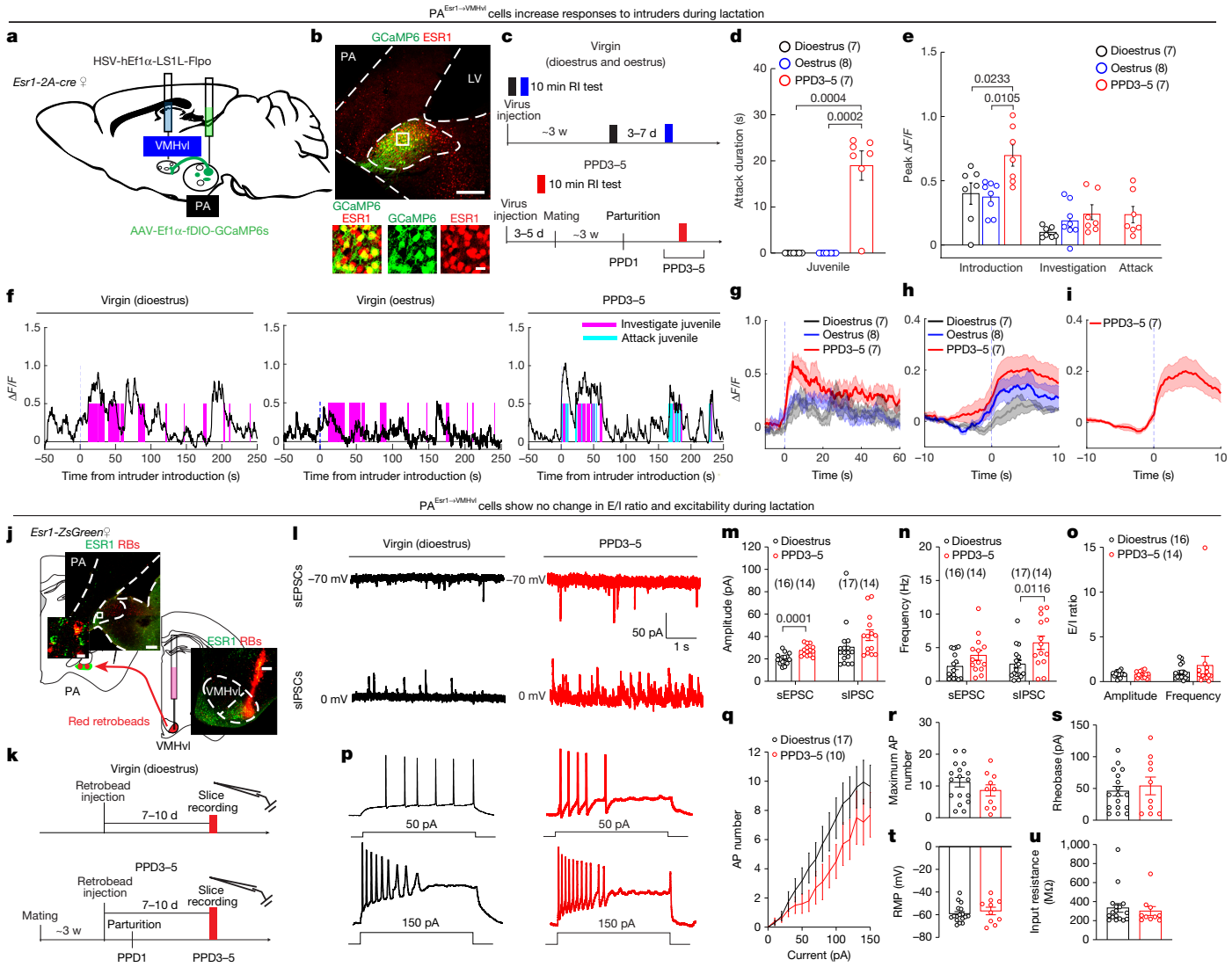

Fig. 3 | Changes in PA$^{Esr1→VMHvl}$ responses to intruders and physiology properties in lactating female mice. a, Experimental schematic. **b**, Representative images showing GCaMP6s (green) and ESR1 (red) expression in the PA. Bottom, magnified views. **c**, Experimental timeline. **d**, The mean attack duration toward juvenile intruders. **e**, Peak Ca^{2+} responses of PA$^{Esr1→VMHvl}$ cells during intruder introduction, investigation and attack. **f**, Representative Ca^{2+} traces during interactions with juvenile intruders in dioestrous (left), oestrous (middle) and lactating (right) female mice. The shaded regions indicate behavioural epochs. **g**–**i**, Peri-event time histograms of the Ca^{2+} signals aligned to intruder introduction (**g**), investigation (**h**) and attack (**i**). **j**, Experimental schematic and representative images showing ESR1 expression (green) and VMHvl-injected retrobeads (red). Left, magnified view. Brain illustrations were adapted from the Allen Brain Reference Atlas (https://atlas.brain-map.org). **k**, Experimental timeline. **l**, Representative voltage-clamp recording traces of PA$^{Esr1→VMHvl}$ cells in dioestrous and lactating female mice. **m**–**o**, The sEPSC and sIPSC amplitude (**m**) and frequency (**n**) and excitatory/inhibitory (E/I) ratio (**o**) of PA$^{Esr1→VMHvl}$ cells in dioestrous and lactating female mice. **p**, Example current-clamp responses to 50 and 150 pA current injections. **q**–**u**, *F*–*I* curves (**q**), the maximum number of action potentials (**r**), rheobase (**s**), RMP (**t**) and input resistance (**u**) of PA$^{Esr1→VMHvl}$ cells in dioestrous (black) and lactating (red) female mice. Data are mean ± s.e.m. The numbers in parentheses denote mice (**d**, **e** and **g**–**i**) or recorded cells (**m**–**o** and **q**–**u**). Statistical analysis was performed using Kruskal–Wallis tests with Dunn's correction (**d** and **e** (investigation)), one-way ANOVA with Tukey's correction (**e** (introduction)), unpaired *t*-tests (**m** (sEPSC), **o** (amplitude) and **r**–**t**), Mann–Whitney *U*-tests (**m** (sIPSC), **n**, **o** (frequency) and **u**) and mixed-effects analysis with repeated measures and Bonferroni correction (**q**). Cells in **m**–**o** and **q**–**u** were recorded from 4 dioestrous and 4 lactating female mice. All *P* values <0.05 are indicated. All tests were two-tailed. Detailed statistics are provided in Supplementary Table 1. Scale bars, 200 µm (**b** (top) and **j** (middle and right)) and 20 µm (**b** (bottom) and **j** (left)).

Ca^{2+} activity using fibre photometry (Fig. 3a). Specifically, we injected HSV-hEf1α-LS1L-Flpo into the VMHvl and AAV-Ef1α-fDIO-GCaMP6s into the PA of C57 *Esr1-2A-cre* × SW F_1 hybrid female mice (Fig. 3a). Histology confirmed that GCaMP6s expression was largely restricted to ESR1$^+$ cells (92.6% cells, $n = 2$ mice; Fig. 3b). As the PA GCaMP6 signal tends to shift over time, probably due to high expression, we recorded PA$^{Esr1→VMHvl}$ cell activity in separate virgin and lactating cohorts with similar virus incubation periods (Fig. 3c). PA$^{Esr1→VMHvl}$ cells showed their strongest activation during intruder introduction, with maximal responses during lactation (Fig. 3e–g). During social investigation, the cells responded moderately, with a trend of higher responses in lactating females (Fig. 3e,h). Moreover, PA$^{Esr1→VMHvl}$ cells consistently increased activity during attack, which occurred exclusively in mothers (Fig. 3d–f,i).

To confirm that enhanced responses were not driven by behavioural differences, we recorded PA$^{Esr1→VMHvl}$ cells in head-fixed awake female mice exposed to social stimuli (Extended Data Fig. 7a). Consistent with free-moving recordings, PA$^{Esr1→VMHvl}$ cells showed significantly higher responses to juveniles, adult males and adult females in lactating females than in dioestrous or oestrous virgins (Extended Data Fig. 7b–e), while minimal responses were observed to objects (Extended

Data Fig. 7b–e). These in vivo data indicate that $PA^{Esr1\rightarrow VMHvl}$ cells also undergo changes during lactation, contributing to increased aggression circuit output.

Next, we performed in vitro patch-clamp recordings of $PA^{Esr1\rightarrow VMHvl}$ cells in brain slices from dioestrous and lactating *Esr1-zsGreen* female mice to examine the cellular basis of these changes. We injected retrobeads into the VMHvl and recorded retrobead-labelled PA cells 7–10 days later (Fig. 3j,k). Both sEPSCs and sIPSCs of $PA^{Esr1\rightarrow VMHvl}$ cells increased moderately during lactation (Fig. 3l–n). Specifically, the sEPSC amplitude and sIPSC frequency were significantly elevated, while the sEPSC frequency and sIPSC amplitude showed increasing trends in lactating females (Fig. 3m,n). Despite these changes, the excitation/inhibition ratio remained unchanged (Fig. 3o). Furthermore, in contrast to $VMHvl^{Npy2r}$ cells, frequency–current (*F–I*) curves revealed no change in $PA^{Esr1\rightarrow VMHvl}$ cell excitability during lactation compared with in the virgin state (Fig. 3p–r). Rheobase, RMP and input resistance were also unchanged (Fig. 3s–u). These data suggest that $PA^{Esr1\rightarrow VMHvl}$ and $VMHvl^{Npy2r}$ cells undergo distinct physiological adaptations during lactation.

Oxytocin modulates aggression through PA

Given a lack of increase in excitability or excitatory/inhibitory ratio of PA cells during lactation, we investigated whether additional mechanisms exist to support increased $PA^{Esr1\rightarrow VMHvl}$ responses to intruders during lactation. Previous studies[22,23] and gene expression database (https://mouse.brain-map.org)[24] indicate high oxytocin receptor (*Oxtr*) expression in the PA. Given the elevated oxytocin levels during lactation and the typical excitatory G_q-mediated effects of OXTR[25], we hypothesized that OXTR signalling may facilitate PA activity during lactation. To test this, we first examined the *Oxtr* expression in the PA using RNAscope-based in situ hybridization[26] and found that almost all PA^{Esr1} cells express *Oxtr* regardless of the reproductive state (Fig. 4a–c). Notably, *Oxtr* expression levels in PA^{Esr1} cells were significantly higher in lactating females, suggesting enhanced oxytocin sensitivity (Fig. 4a,c). We next examined the effect of oxytocin on PA^{Esr1} cell activity in lactating females using in vitro current-clamp recording (Fig. 4d). Application of TGOT, a selective OXTR agonist, significantly increased input resistance without altering the RMP (Fig. 4e,f). In the presence of TGOT, PA^{Esr1} cells fired more action potentials in response to 50 or 100 pA current injection (Fig. 4g–i), indicating that oxytocin enhances PA^{Esr1} input–output gain.

To assess the functional role of PA OXTR signalling in maternal aggression, we injected saline or an OXTR antagonist (OXTRA; L-371,257, 100 μM, 250 nl per side) into the PA of lactating female mice 30 min before intruder introduction (Fig. 4j). After OXTRA injection, C57 × SW F_1 hybrid females attacked the intruder less frequently and with longer latency compared with saline injection, while investigation duration remained unchanged (Fig. 4k–m). Similar reductions in aggression were observed in SW mothers after PA OXTRA injection (Extended Data Fig. 8).

We further deleted *Oxtr* in the PA by bilaterally injecting *cre-GFP* virus into $Oxtr^{flox/flox}$ female mice on the SW and C57 mixed background ($Oxtr^{PA\text{-}KO}$)[27] (Fig. 4n). Controls received GFP virus ($Oxtr^{PA\text{-}GFP}$). Compared with the controls, $Oxtr^{PA\text{-}KO}$ female mice showed a reduced attack duration and prolonged latency, with no change in investigation time (Fig. 4o–q). Together, these manipulations demonstrate that PA OXTR signalling promotes maternal aggression.

Oxtr is also highly expressed in the VMHvl and is upregulated during lactation (Extended Data Fig. 9a,b). By contrast, *Esr1* expression is unchanged, whereas *Npy2r* expression decreases (Extended Data Fig. 9a,b). However, *Oxtr* is not enriched in aggression-related VMHvl cells: only 28% of *Npy2r*-positive cells express *Oxtr* in oestrous female mice, and this proportion decreases to 18% during lactation (Extended Data Fig. 9c,d). In contrast to effects of PA OXTR manipulation, neither OXTRA injection nor conditional *Oxtr* deletion in the VMHvl significantly altered maternal aggression, indicating that OXTR modulates maternal aggression primarily through the PA rather than the VMHvl (Extended Data Fig. 9e-l).

Oxytocin links pup to maternal attack

As maternal aggression serves to protect the young, females adjust this energetically costly behaviour to pup needs. During the first postpartum week, when pups are most vulnerable to infanticide, maternal aggression peaks[1,2,5] (Supplementary Note 1). In scenarios in which pups no longer exist, for example, due to predation or illness, maternal aggression rapidly declines[2,5]. Consistent with previous studies[28,29], we found that female aggression significantly decreased 24 h after pup removal and was restored 24 h after reunion (Fig. 5a,c,d). Serum oxytocin levels closely tracked maternal aggression changes, decreasing after pup separation and increasing after reunion (Fig. 5b). This is not surprising given that oxytocin is released during nursing, which requires pup presence[30–32].

To test whether decreased oxytocin underlies the drop in maternal aggression after pup separation, we optogenetically activated oxytocin neurons in the paraventricular hypothalamic nucleus (PVN^{Oxt}), which are the primary source of oxytocin and are highly activated during pup interaction[30,31,33]. We virally expressed ChR2 (GFP control) in PVN cells of C57 *Oxt-ires-cre* × SW F_1 hybrid virgin female mice, which were later paired and became mothers (Fig. 5e). On PPD3, we assessed aggression using a juvenile intruder, removed pups for 24 h and retested aggression (Fig. 5f). As expected, both GFP and ChR2 females attacked the intruder before separation and showed markedly reduced aggression afterwards (Fig. 5h,i). We then delivered light stimulation (5 mW, 20 Hz, 20 ms; 20 s on, 40 s off) for 1 h, which significantly elevated serum oxytocin (Fig. 5g). Notably, aggression in ChR2 female mice recovered to preseparation levels, whereas GFP female mice remained largely non-aggressive (Fig. 5h,i). Given the critical role of PA OXTR signalling in promoting maternal aggression, we next examined whether PVN^{Oxt}-induced recovery depends on PA OXTR (Fig. 5j). OXTRA, but not saline, injected into the PA fully blocked the aggression recovery after PVN^{Oxt} stimulation (Fig. 5k,l).

Consistent with the behavioural results, Ca^{2+} responses of VMHvl-projecting PA cells to juvenile intruders were significantly reduced after 24 h of pup separation (Fig. 5m–r). One hour of PVN^{Oxt} stimulation restored these responses to pre-separation levels (Fig. 5m–r). These findings indicate that oxytocin release from PVN^{Oxt} neurons activates PA OXTR signalling, enhancing PA output and facilitating maternal aggression.

Importantly, the aggression circuit does not revert to the virgin state after 24 h of pup separation. PA *Oxtr* expression remained elevated 1 day after separation (Fig. 5s–u), indicating sustained oxytocin sensitivity. Moreover, optogenetic activation of $PA^{Esr1\rightarrow VMHvl}$ terminals continued to elicit time-locked attacks, suggesting that PA–VMHvl connectivity and $VMHvl^{Npy2r}$ excitability remain potentiated (Extended Data Fig. 10). This circuit stability allows rapid reinstatement of maternal aggression after pup return. Together, these results suggest that oxytocin conveys information about pup presence and developmental stage to dynamically gate maternal aggression, ensuring robust expression only when needed.

Discussion

Female aggression increases abruptly after childbirth in mammals to protect offspring, which requires enhanced output from the neural circuits of aggression. We identified PA^{Esr1} cells as an essential upstream population of the $VMHvl^{Npy2r}$ cells in the promotion of aggression. During lactation, the PA^{Esr1}–$VMHvl^{Npy2r}$ circuit undergoes synaptic and cellular adaptations that enhance $VMHvl^{Npy2r}$ responses to intruders,

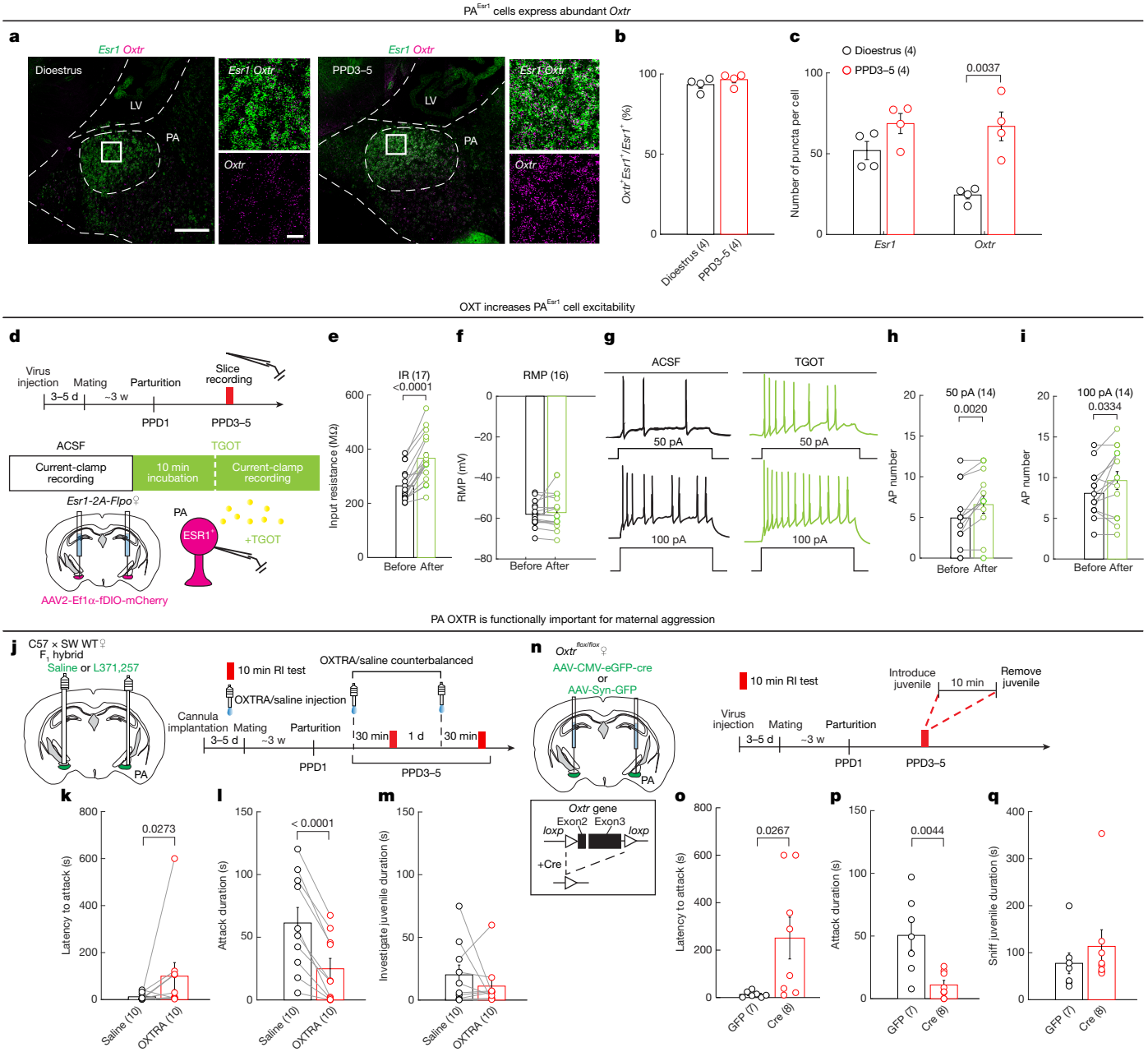

Fig. 4 | OXTR promotes maternal aggression by enhancing PA activity. **a**, Representative images showing *Oxtr* (magenta) and *Esr1* (green) mRNA in the PA of dioestrous and lactating female mice. Right, magnified views of the areas indicated by boxes. **b**, The percentage of PA^{Esr1} cells expressing *Oxtr*. **c**, The number of *Esr1* and *Oxtr* mRNA puncta per expressing cell in the PA of dioestrous and lactating female mice. **d**, Experimental schematics and timeline. **e**,**f**, Input resistance (**e**) and RMP (**f**) of PA^{Esr1} cells in lactating female mice before and after application of TGOT—a selective OXTR agonist. **g**, Example current-clamp recording traces in response to 50 and 100 pA current injections before and after TGOT application. **h**,**i**, The number of spikes evoked by 50 pA (**h**) and 100 pA (**i**) current injections before and after TGOT perfusion. **j**, Experimental schematics and timeline. **k**–**m**, The latency to attack (**k**), attack duration (**l**) and intruder investigation duration (**m**) after injecting saline or L-371,257 hydrochloride, a potent OXTRA. **n**, Experimental schematics and timeline. **o**–**q**, The latency to attack (**o**), attack duration (**p**) and intruder investigation duration (**q**) in GFP- and Cre-injected mice. The attack latency was set to 600 s if no attack occurred. Data are mean ± s.e.m. The numbers in parentheses indicate the number of mice (**b**, **c**, **k**–**m** and **o**–**q**) and recorded cells (**e**, **f**, **h** and **i**). Statistical analysis was performed using unpaired *t*-tests (**b**, **c**, **o** and **p**), Wilcoxon matched-pairs signed rank tests (**e**, **k** and **m**), paired *t*-tests (**f**, **h**, **i** and **l**) and Mann–Whitney *U*-tests (**q**). Cells in **e**, **f**, **h** and **i** were recorded from four lactating female mice. All *P* values <0.05 are indicated. All tests were two-tailed. Detailed statistics are provided in Supplementary Table 1. Brain illustrations in **d**, **j** and **n** were adapted from the Allen Brain Reference Atlas (https://atlas.brain-map.org). Scale bars, 200 µm (**a**, main images) and 20 µm (**a**, insets).

driving aggression. Moreover, PA^{Esr1} cells express abundant *Oxtr*, enabling oxytocin to further amplify PA output. As oxytocin release is tightly coupled to pup suckling, and therefore to pup presence and developmental stage, PA^{Esr1} activity can be dynamically regulated by offspring status, ensuring that maternal aggression is expressed only when needed to protect the young (Fig. 5v).

Plasticity of the PA-to-VMHvl pathway

The VMHvl is well established as a key region for social behaviours. In female mice, two VMHvl subpopulations marked by *Npy2r* and *Cckar* selectively govern aggressive and sexual behaviours, respectively[13–15]. Our study of VMHvl^{Npy2r} cells, together with our recent work

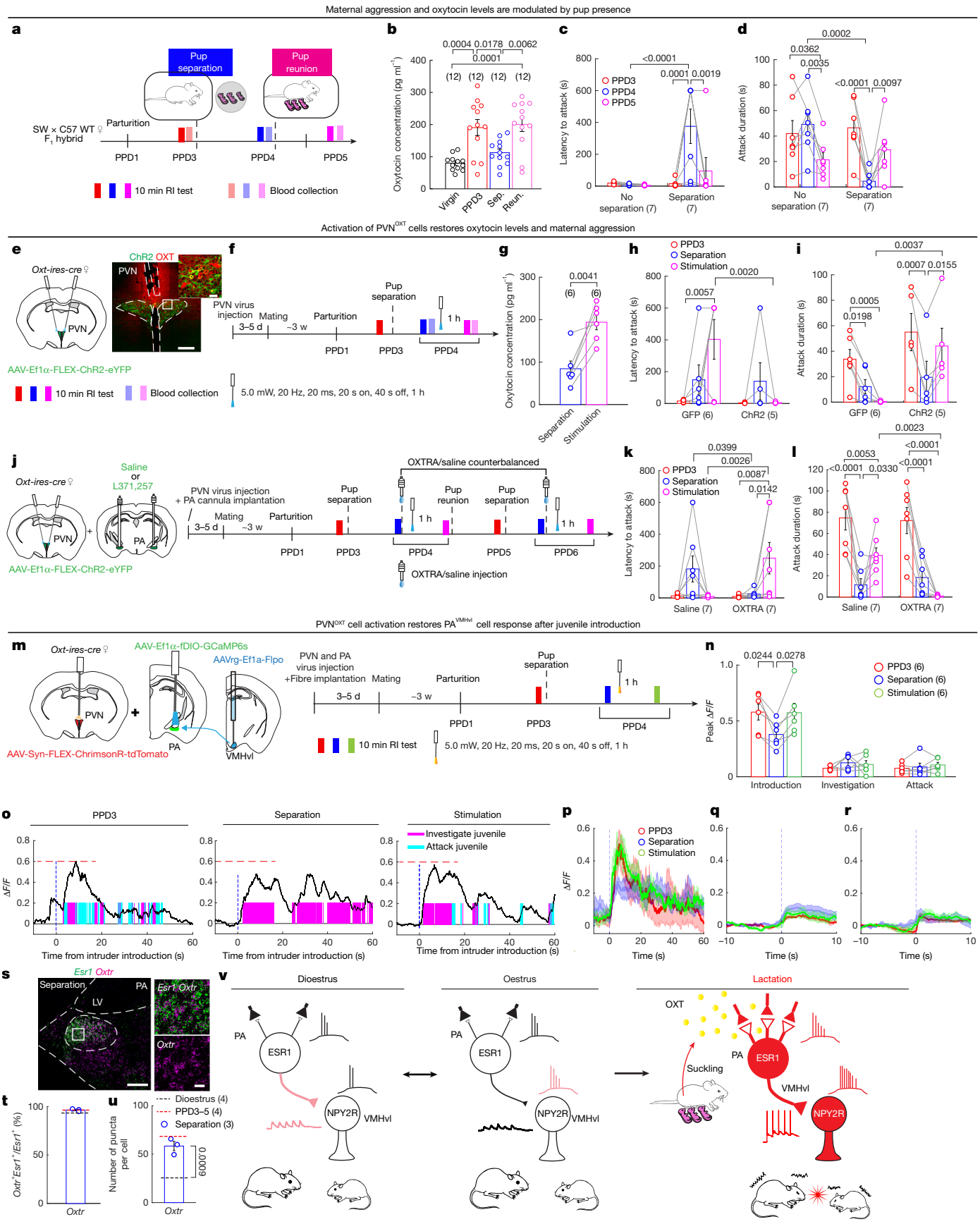

Fig. 5 | See next page for caption.

Fig. 5 | Pup-dependent oxytocin release maintains maternal aggression. **a**, Experimental schematic testing the effect of pup separation (sep.) on maternal aggression. Blood collection and RI tests were performed in separate animals. **b**, The serum oxytocin levels in virgin females (black), PPD3 females (red), PPD4 females 24 h after pup separation (blue) and PPD5 females 24 h after pup reunion (reun.; magenta). **c**,**d**, The attack latency (**c**) and attack duration (**d**) in PPD3–PPD5 female mice. For separation group, pups were removed after PPD3 testing and returned after PPD4 testing. The latency was set to 600 s if no attack occurred. **e**, Schematic and histology showing ChR2 expression and OXT staining. Right, enlarged view. **f**, Experiment timeline testing the effect of PVN^{Oxt} activation on maternal aggression after pup separation. **g**, Serum oxytocin levels in PPD4 female mice after 24 h pup separation before (blue) and after (magenta) PVN^{Oxt} stimulation. **h**,**i**, The attack latency (**h**) and attack duration (**i**) in PPD3 and PPD4 female mice after 24 h pup separation before and after PVN^{Oxt} light delivery in the ChR2 and GFP groups. **j**, Experimental schematic for testing the effect of PA OXTR antagonism in PVN^{Oxt}-stimulation-induced recovery of maternal aggression. **k**,**l**, The attack latency (**k**) and duration (**l**) in PPD3 and PPD4 female mice after 24 h pup separation, before and after PVN^{Oxt} stimulation in the PA OXTRA- and saline-injected groups. **m**, Experimental schematic for examining the effect of PVN^{Oxt} stimulation on PA^{VMHvl} Ca^{2+} responses to juvenile intruders after pup separation. **n**, The peak Ca^{2+} signals of PA^{VMHvl} cells during intruder introduction, investigation and attack. **o**, Representative Ca^{2+} traces of PA^{VMHvl} cells during juvenile intruder interaction in PPD3 female mice (left) and PPD4 female mice after pup separation before (middle) and after (right) 1 h PVN^{Oxt} cell activation. The shaded regions denote behavioural epochs. The dashed red line indicates $\Delta F/F = 0.6$. **p**–**r**, Peri-event time histograms of the Ca^{2+} signal of PA^{VMHvl} cells aligned to intruder introduction (**p**), investigation (**q**) and attack (**r**). **s**, Representative RNAscope images showing *Oxtr* (magenta) and *Esr1* (green) expression in the PA of a pup-separated lactating female. Right, magnified view. **t**,**u**, The percentage of PA^{Esr1} cells expressing *Oxtr* (**t**) and the number of *Oxtr* puncta per expressing cell (**u**) in lactating female mice after 24 h pup separation. The dashed lines indicate average values in virgin (black) and lactating (red) female mice. **v**, Model summarizing circuit plasticity underlying maternal aggression. During lactation, strengthened PA-to-$VMHvl^{Npy2r}$ connectivity and increased $VMHvl^{Npy2r}$ excitability enhance aggression. Pup-dependent oxytocin release further amplifies PA^{Esr1} output, enabling rapid and reversible adjustment of aggression according to pup-protection needs. Data are mean ± s.e.m. The numbers indicate mice. Statistical analysis was performed using one-way ANOVA with Tukey correction (**b**), mixed-effects analysis with repeated measures and Bonferroni correction (**c**,**d**,**h**,**i**,**k** and **l**), paired *t*-tests (**g**), repeated-measures one-way ANOVA with Tukey correction (introduction, investigation) or Friedman test with Dunn correction (attack) (**n**), and unpaired *t*-tests (**t** and **u**). All tests were two-sided. All *P* values <0.05 are shown. Detailed statistics are provided in Supplementary Table 1. Brain illustrations in **e**, **j** and **m** were adapted from the Allen Brain Reference Atlas (https://atlas.brain-map.org). Scale bars, 200 μm (**e** and **s** (left)) and 20 μm (**e** and **s** (right)).

on $VMHvl^{Cckar}$ cells[15], revealed their differential connections with PA and distinct reproductive state-dependent plasticity. In virgin female mice, sexual receptivity is high during oestrus and low during dioestrus. Accordingly, $VMHvl^{Cckar}$ cells exhibit greater excitability and reduced inhibitory synaptic input during oestrus compared with dioestrus[15]. In most laboratory mouse strains, aggression in virgin female mice remains low across oestrous stages, yet we identified oestrous-state-dependent physiological differences in the aggression circuit. During dioestrus, PA-$VMHvl^{Npy2r}$ connection probability is relatively high, but $VMHvl^{Npy2r}$ cell excitability is low. By contrast, during oestrus, $VMHvl^{Npy2r}$ cell excitability is relatively high, but PA-$VMHvl^{Npy2r}$ connections are nearly absent. The mechanisms driving these cycle-dependent synaptic and cellular changes remain unclear, but either reduced excitability or weak synaptic input would constrain aggression circuit activation in virgin females. These oestrous-cycle-dependent circuit changes suggest that, if the aggression circuit were more active, virgin females might exhibit cycle-dependent variation in aggression. Consistent with this, female California mice and rats display higher aggression during dioestrus than during proestrus–oestrus[34,35].

Notably, the PA provides almost no input to mating-related $VMHvl^{Npy2r(-)Esr1(+)}$ cells during oestrus, despite the dense PA terminals in the VMHvll. Behaviourally, manipulating the PA-to-VMHvl pathway does not alter female sexual behaviours, indicating that VMHvl-mediated female sexual receptivity operates independently of PA inputs. Consistent with this, $VMHvl^{Cckar}$ and $VMHvl^{Npy2r(-)Esr1(+)}$ cells show low sEPSC frequencies, especially compared with aggression-related $VMHvl^{Npy2r}$ cells (Fig. 2m and Extended Data Fig. 6q). This weak reliance on excitatory input suggests that sexual receptivity is governed primarily by hormonal state rather than external drive. Indeed, in female rats that are 'in heat', minimal stimulation, such as a light touch on the back, is sufficient to elicit lordosis[36].

During lactation, the excitability of $VMHvl^{Cckar}$ cells is low (maximum firing rate of around 5 Hz)[15], while $VMHvl^{Npy2r}$ cell excitability becomes high (maximum firing rate of 10 Hz). Moreover, PA-to-$VMHvl^{Npy2r}$ cell connectivity is strengthened, with more $VMHvl^{Npy2r}$ cells receiving PA input, while PA becomes largely disconnected from $VMHvl^{Npy2r(-)Esr1(+)}$ cells. Consequently, the PA can effectively drive $VMHvl^{Npy2r}$ cells without engaging mating-related VMHvl cells. This segregation is probably important, as mating-related VMHvl cells appear to antagonize aggression-related VMHvl cells[15]. Indeed, during lactation, activation of $VMHvl^{Cckar}$ cells suppresses maternal aggression despite unchanged sexual receptivity[15].

After 24 h of pup separation, natural maternal aggression was reduced; however, PA^{Esr1}-to-VMHvl terminal stimulation still effectively promoted attack, indicating that $VMHvl^{Npy2r}$ cell excitability and PA^{Esr1}-to-VMHvl synaptic strength probably remain high. These sustained circuit properties probably enable rapid reinstatement of aggression after pup return. We speculate that PA^{Esr1}–VMHvl circuit remodelling is induced by pregnancy-associated hormone changes and is largely independent of oxytocin levels during lactation. The molecular mechanisms underlying enhanced $VMHvl^{NPY2r}$ excitability and strengthened PA-to-VMHvl connectivity remain important topics for future investigation.

Comparing male and female aggression circuits

The PA^{Esr1}–$VMHvl^{Esr1}$ circuit is also essential for male aggression, and direct comparison across sexes provides insights into sex differences in aggressive behaviour. In males, most (around 80%) $VMHvl^{Esr1}$ cells receive excitatory PA input even without prior fighting experience[16]. By contrast, PA input to $VMHvl^{Npy2r}$ cells in virgin females is sparse and oestrous-state dependent, reaching around 10% in oestrus and around 65% in dioestrus. During lactation, this proportion rises to about 80%, comparable to naive males.

Beyond synaptic connectivity, intrinsic excitability also differs between sexes. The rheobase of $VMHvl^{Npy2r}$ cells in virgin females is higher than that of $VMHvl^{Esr1}$ cells in naive males[19], meaning that female aggression-related VMHvl cells require stronger excitatory drive to reach spiking threshold. Together with stronger PA inputs, lower firing thresholds and a larger number of aggression-related VMHvl cells in males (note that only about half of female $VMHvl^{Esr1}$ cells contribute to aggression[11]), these features probably make attack behaviour more readily initiated in males than in females.

Oxytocin dynamically signals the need to protect pups

Maternal aggression is unique in that its primary function is to protect offspring. Accordingly, its intensity must closely track pup needs, ensuring females avoid unnecessary and potentially dangerous conflicts. Here we identify oxytocin as a key mediator linking pup needs to aggression-circuit output. High oxytocin levels maintained by suckling are essential for sustaining robust maternal aggression.

During lactation, *Oxtr* expression markedly increases in the VMHvl, PA and many other limbic regions, probably driven by ESR1 activation after the pregnancy-associated oestrogen surge[37,38]. Notably, PA,

rather than VMHvl, emerges as the critical site where oxytocin enhances aggression-circuit output. In the PA, *Oxtr* is broadly and strongly expressed in nearly all PA^{Esr1} cells, allowing oxytocin to increase the input–output gain of the cells by elevating input resistance, potentially through the closure of certain potassium channels[39]. As this effect builds slowly, it may account for the slow decline in maternal aggression after pup separation and the moderate suppression observed after acute PA OXTR antagonism.

In contrast to oxytocin's role in synaptic plasticity, which can induce long-lasting circuit changes, the effect of oxytocin on PA neurons appears to require its continued presence. This feature probably allows oxytocin to couple PA output to pup needs with high temporal fidelity. Notably, after *Oxtr* knockout in the PA, maternal aggression is heavily suppressed but not eliminated. The remaining aggression probably reflects an amplifying rather than an absolute gating role of oxytocin: even in the absence of oxytocin, PA input can still drive VMHvl activity to some degree.

Oxtr is also abundantly expressed in the male PA, raising the possibility that oxytocin modulates aggression in fathers. This seems plausible in biparental species such as California mice, in which males display heightened paternal aggression[40]. Although males do not nurse, oxytocin can be released during infant interactions[41]. Supporting this idea, excitatory input from the lateral hypothalamus to PVN^{Oxt} neurons is strengthened in fathers compared with in virgin males[42], providing a potential mechanism for increased oxytocin release during fatherhood. However, a recent study in wild mice reported a sexually dimorphic role of oxytocin in aggression: it promotes interfemale aggression while having no detectable effect on intermale aggression[43]. Whether male house mice (*Mus musculus*) display parenthood-associated aggression and whether PA oxytocin signalling contributes to such behaviours remain open questions.

Oxytocin in the PA may arise from sparse direct projections of PVN^{Oxt} neurons[44], but PA neurons may also detect oxytocin in the cerebrospinal fluid, given their proximity to the lateral ventricle. Indeed, CSF oxytocin levels increase during suckling[45]. As maternal aggression does not fluctuate on rapid timescales, the slower dynamics of CSF oxytocin should suffice to convey pup need. Importantly, this mode of regulation is reversible: oxytocin levels rise rapidly after pup reunion, and maternal aggression is promptly restored.

In the VMHvl, OXTR signalling may have functions unrelated to female aggression. Our recent work showed that oxytocin originating from the retrochiasmatic supraoptic nucleus promotes social avoidance learning after defeat by enhancing synaptic potentiation of anterior VMHvl^{OXTR} cells in both male and female mice[46]. Nonetheless, VMHvl oxytocin may still contribute to aggression in males, as simultaneous mutation of oxytocin and vasopressin receptors in VMHvl^{Esr1} cells suppresses male aggression[47].

Our study reveals the neural mechanisms underlying the distinctive dynamics of female mouse aggression during motherhood. Synaptic and cellular changes, probably triggered by the surge of sex hormones during pregnancy and parturition, prime the aggression circuit for rapid engagement, while oxytocin provides an additional layer of control to ensure aggression is deployed appropriately to protect the young. Together, these mechanisms allow the mother to attack intruders vigorously on first encounter while rapidly and reversibly adjusting her aggression level in response to her offspring's needs.

Online content

Any methods, additional references, Nature Portfolio reporting summaries, source data, extended data, supplementary information, acknowledgements, peer review information; details of author contributions and competing interests; and statements of data and code availability are available at https://doi.org/10.1038/s41586-026-10354-5.

1. John, R. D. S. & Corning, P. A. Maternal aggression in mice. *Behav. Biol.* **9**, 635–639 (1973).
2. Lonstein, J. S. & Gammie, S. C. Sensory, hormonal, and neural control of maternal aggression in laboratory rodents. *Neurosci. Biobehav. Rev.* **26**, 869–888 (2002).
3. Caughey, S. D. et al. Changes in the intensity of maternal aggression and central oxytocin and vasopressin V1a receptors across the peripartum period in the rat. *J. Neuroendocrinol.* **23**, 1113–1124 (2011).
4. Svare, B. & Gandelman, R. Postpartum aggression in mice: experiential and environmental factors. *Horm. Behav.* **4**, 323–334 (1973).
5. Bosch, O. J. Maternal aggression in rodents: brain oxytocin and vasopressin mediate pup defence. *Philos. Trans. R Soc. Lond. B* **368**, 20130085 (2013).
6. Svare, B. B. & Mann, M. A. in *Hormones and Aggressive Behavior* (ed. Svare, B. B.) 91–104 (Springer, 1983).
7. Svare, B. & Gandelman, R. Suckling stimulation induces aggression in virgin female mice. *Nature* **260**, 606–608 (1976).
8. Svare, B. & Gandelman, R. Postpartum aggression in mice: the influence of suckling stimulation. *Horm. Behav.* **7**, 407–416 (1976).
9. Lin, D. et al. Functional identification of an aggression locus in the mouse hypothalamus. *Nature* **470**, 221–226 (2011).
10. Lee, H. et al. Scalable control of mounting and attack by Esr1^{+} neurons in the ventromedial hypothalamus. *Nature* **509**, 627–632 (2014).
11. Hashikawa, K. et al. Esr1^{+} cells in the ventromedial hypothalamus control female aggression. *Nat. Neurosci.* **20**, 1580–1590 (2017).
12. Hashikawa, K., Hashikawa, Y., Lischinsky, J. & Lin, D. The neural mechanisms of sexually dimorphic aggressive behaviors. *Trends Genet.* **34**, 755–776 (2018).
13. Liu, M., Kim, D. W., Zeng, H. & Anderson, D. J. Make war not love: the neural substrate underlying a state-dependent switch in female social behavior. *Neuron* **110**, 841–856 (2022).
14. Knoedler, J. R. et al. A functional cellular framework for sex and estrous cycle-dependent gene expression and behavior. *Cell* **185**, 654–671 (2022).
15. Yin, L. et al. VMHvll^{Cckar} cells dynamically control female sexual behaviors over the reproductive cycle. *Neuron* **110**, 3000–3017 (2022).
16. Yamaguchi, T. et al. Posterior amygdala regulates sexual and aggressive behaviors in male mice. *Nat. Neurosci.* **23**, 1111–1124 (2020).
17. Zha, X. et al. VMHvl-projecting Vglut1^{+} neurons in the posterior amygdala gate territorial aggression. *Cell Rep.* **31**, 107517 (2020).
18. Stagkourakis, S., Spigolon, G., Liu, G. & Anderson, D. J. Experience-dependent plasticity in an innate social behavior is mediated by hypothalamic LTP. *Proc. Natl Acad. Sci. USA* **117**, 25789–25799 (2020).
19. Yan, R. et al. The multi-stage plasticity in the aggression circuit underlying the winner effect. *Cell* https://doi.org/10.1016/j.cell.2024.09.030 (2024).
20. Yin, L. & Lin, D. Neural control of female sexual behaviors. *Horm. Behav.* **151**, 105339 (2023).
21. Inoue, S. et al. Periodic remodeling in a neural circuit governs timing of female sexual behavior. *Cell* **179**, 1393–1408 (2019).
22. Yoshida, M. et al. Evidence that oxytocin exerts anxiolytic effects via oxytocin receptor expressed in serotonergic neurons in mice. *J. Neurosci.* **29**, 2259–2271 (2009).
23. Li, H. et al. Spatiotemporal mapping of the oxytocin receptor at single-cell resolution in the postnatally developing mouse brain. *Neurosci. Bull.* https://doi.org/10.1007/s12264-024-01296-x (2024).
24. Lein, E. S. et al. Genome-wide atlas of gene expression in the adult mouse brain. *Nature* **445**, 168–176 (2007).
25. Jurek, B. & Neumann, I. D. The oxytocin receptor: from intracellular signaling to behavior. *Physiol. Rev.* **98**, 1805–1908 (2018).
26. Wang, F. et al. RNAscope: a novel in situ RNA analysis platform for formalin-fixed, paraffin-embedded tissues. *J. Mol. Diagn.* **14**, 22–29 (2012).
27. Lee, H. J., Caldwell, H. K., Macbeth, A. H., Tolu, S. G. & Young, W. S. 3rd. A conditional knockout mouse line of the oxytocin receptor. *Endocrinology* **149**, 3256–3263 (2008).
28. Gandelman, R. Mice: postpartum aggression elicited by the presence of an intruder. *Horm. Behav.* **3**, 23–28 (1972).
29. Flannelly, K. J. & Kemble, E. D. The effect of pup presence and intruder behavior on maternal aggression in rats. *Bull. Psychon. Soc.* **25**, 133–135 (1987).
30. Froemke, R. C. & Young, L. J. Oxytocin, neural plasticity, and social behavior. *Annu. Rev. Neurosci.* **44**, 359–381 (2021).
31. Yukinaga, H. et al. Recording and manipulation of the maternal oxytocin neural activities in mice. *Curr. Biol.* **32**, 3821–3829 (2022).
32. Neumann, I., Russell, J. A. & Landgraf, R. Oxytocin and vasopressin release within the supraoptic and paraventricular nuclei of pregnant, parturient and lactating rats: a microdialysis study. *Neuroscience* **53**, 65–75 (1993).
33. Yaguchi, K. et al. Dynamic modulation of pulsatile activities of oxytocin neurons in lactating wild-type mice. *PLoS ONE* **18**, e0285589 (2023).
34. Oliveira, V. E. M. et al. Oxytocin and vasopressin within the ventral and dorsal lateral septum modulate aggression in female rats. *Nat. Commun.* **12**, 2900 (2021).
35. Davis, E. S. & Marler, C. A. The progesterone challenge: steroid hormone changes following a simulated territorial intrusion in female *Peromyscus californicus*. *Horm. Behav.* **44**, 185–198 (2003).
36. Kow, L. M., Montgomery, M. O. & Pfaff, D. W. Triggering of lordosis reflex in female rats with somatosensory stimulation: quantitative determination of stimulus parameters. *J. Neurophysiol.* **42**, 195–202 (1979).
37. Young, L. J., Wang, Z., Donaldson, R. & Rissman, E. F. Estrogen receptor α is essential for induction of oxytocin receptor by estrogen. *Neuroreport* **9**, 933–936 (1998).
38. Insel, T. R. Postpartum increases in brain oxytocin binding. *Neuroendocrinology* **44**, 515–518 (2008).
39. Liu, J. J., Eyring, K. W., Konig, G. M., Kostenis, E. & Tsien, R. W. Oxytocin-modulated ion channel ensemble controls depolarization, integration and burst firing in CA2 pyramidal neurons. *J. Neurosci.* **42**, 7707–7720 (2022).

40. Trainor, B. C., Finy, M. S. & Nelson, R. J. Paternal aggression in a biparental mouse: parallels with maternal aggression. *Horm. Behav.* **53**, 200–207 (2008).
41. Morris, A. R. et al. Physical touch during father-infant interactions is associated with paternal oxytocin levels. *Infant Behav. Dev.* **64**, 101613 (2021).
42. Inada, K. et al. Plasticity of neural connections underlying oxytocin-mediated parental behaviors of male mice. *Neuron* **110**, 2009–2023.e2005 (2022).
43. Sofer, Y. et al. Sexually dimorphic oxytocin circuits drive intragroup social conflict and aggression in wild house mice. *Nat. Neurosci.* **27**, 1565–1573 (2024).
44. Li, H. et al. Single-neuron projectomes of mouse paraventricular hypothalamic nucleus oxytocin neurons reveal mutually exclusive projection patterns. *Neuron* **112**, 1081–1099 e1087 (2024).
45. Nowak, R. et al. Neonatal suckling, oxytocin, and early infant attachment to the mother. *Front. Endocrinol.* **11**, 612651 (2020).
46. Osakada, T. et al. A dedicated hypothalamic oxytocin circuit controls aversive social learning. *Nature* **626**, 347–356 (2024).
47. Mountoufaris, G. et al. A line attractor encoding a persistent internal state requires neuropeptide signaling. *Cell* https://doi.org/10.1016/j.cell.2024.08.015 (2024).

Methods

Mice

All procedures were approved by the New York University Langone Medical Center Institutional Animal Care and Use Committee in compliance with the US National Institutes of Health Guidelines for the Care and Use of Laboratory Animals. Adult mice 12–38 weeks old were used for all of the studies. Mice were housed at 18–23 °C with 40–60% humidity under a 12 h–12 h light–dark cycle (dark cycle, 22:00 to 10:00), with food and water available ad libitum. For C57 and SW mixed-background mice, we bred the F_1 mixed-background mice by crossing a male C57BL/6N (Charles River, 027), C57 *Esr1-2A-cre* (Jackson, 017911), *Esr1-2A-Flpo* (Jackson, 037009), *Npy2r-ires-cre* (Jackson, 029285), or *Oxt-ires-cre* (Jackson, 024234) with a female SW (Taconic, SW-F) mouse. For mixed-background *Npy2r-ires-cre/Esr1-2A-Flpo* double transgenic female mice, we bred the F_3 mixed-background mice by crossing F_2 mixed-background homozygous *Npy2r-ires-cre* female mice with C57 homozygous *Esr1-2A-Flpo* male mice. For hybrid $Oxtr^{flox/flox}$ female mice (Jackson, 008471), we bred the F_2 mixed-background mice by crossing F_1 SW and C57 mixed background $Oxtr^{flox/+}$ *mice*. These mixed-background breeding strategies enabled cell-type-specific manipulations in aggressive lactating female mice. C57 *Esr1-ZsGreen* mice were generated and provided by the Y. Xu lab originally and then bred in-house. Stimulus animals were adult (>8 weeks old) and juvenile (15 days old in one case, and 19–28 days old in all other cases) C57BL/6N female and male mice, originally purchased from Charles River and then bred in-house. Stimulus animals were group-housed. After surgery, all test virgin animals were singly housed, and all lactating animals were co-housed with their pups except during the pup-separation procedure. All experiments were performed during the dark cycle (10:00 to 16:00) of the animals.

Viruses

AAV2-CAG-FLEX-GFP (4.00×10^{12} viral genomes (vg) per ml), AAV2-hSyn-GFP (7.30×10^{12} vg per ml), AAV2-Ef1α-DIO-ChR2-eYFP (4.00×10^{12} vg per ml), AAV5-hSyn-Chronos-GFP (2.10×10^{13} vg per ml) and AAV2-Syn-Flex-ChrimsonR-tdTomato (6.00×10^{12} vg per ml) viruses were purchased from the University of North Carolina vector core. AAV1-CMV-Hl-eGFP-cre (2.63×10^{13} vg per ml), AAV2-Ef1α-DIO-hM4Di-mCherry (5.00×10^{12} vg per ml), AAV2-Ef1α-fDIO-mCherry (8.60×10^{12} vg per ml), AAV8-Ef1α-fDIO-GCaMP6s (1.80×10^{13} vg per ml), AAVrg-Ef1α-Flpo (7×10^{12} vg per ml) and AAV8-Ef1α-Coff/Fon-mCherry[48] (2.00×10^{13} vg per ml) were purchased from Addgene. AAV2-CAG-FLEX-GCaMP6f-WPRE-SV40 (2.27×10^{13} vg per ml) was custom-made by the University of Pennsylvania vector core facility. AAVDJ-Ef1α-fDIO-hM4Di-mCherry (2.65×10^{13} vg per ml) was custom-made by Vigene Biosciences, and the plasmid was provided by B. Lim at USCD. HSV-hEf1α-LS1L-Flpo (1.00×10^{9} vg per ml) was purchased from the Massachusetts General Hospital Neuroscience Center vector core.

Drugs

For chemogenetic inhibition, 5 mg per kg CNO (Sigma-Aldrich, C0832) dissolved in saline was administered i.p. To block OXTRs in the PA and VMHvl, 250 nl per side of 100 μM L-371,257 hydrochloride (Tocris, 2410) in saline was bilaterally injected through the implanted cannulae.

Stereotaxic surgery

Mice (12–20 weeks old) were anaesthetized with isoflurane (1–1.5%) and secured in a stereotaxic apparatus (Kopf Instruments, Model 1900). Viruses and tracers were delivered into the targeted brain regions as previously described[16,49]. In brief, injections were performed using glass capillaries and a nanoinjector (World Precision Instruments, Nanoliter) at rates of 10 nl min^{-1} for viruses and 5 nl min^{-1} for tracers. Only animals with correctly verified injection sites were included in the final analysis ($n = 176$ out of 194).

For retrograde tracing experiments, 50 nl of Alexa-Fluor-555-conjugated CTB (Thermo Fisher Scientific, C22843) was unilaterally injected into the VMHvl (bregma coordinates: anteroposterior (AP) −1.45 mm; mediolateral (ML) ±0.680 mm; dorsoventral (DV) −5.680 mm). Brains were collected 10 days later. Only mice with confirmed targeting of the VMHvl were included in the final analysis ($n = 5$ out of 8).

For pharmacogenetic inhibition of PA^{Esr1} cells, 120 nl of AAV2-hSyn-DIO-hM4Di-mCherry was bilaterally injected into the PA of *Esr1-2A-cre* mice (bregma coordinates: AP, −2.30 mm; ML, ±2.40 mm; DV, −4.80 mm). Only animals with confirmed bilateral targeting of the PA were included in the final analysis ($n = 7$ out of 8).

For pharmacogenetic inhibition of $PA^{Esr1 \rightarrow VMHvl}$ cells, 130 nl of HSV-hEf1α-LS1L-Flpo was injected into the VMHvl while 120 nl of AAVDJ-Ef1α-fDIO-hM4Di-mCherry was injected into the PA bilaterally of *Esr1-2A-cre* mice. Control *Esr1-2A-cre* animals were bilaterally injected with 130 nl of HSV-hEf1α-LS1L-Flpo into the VMHvl and 100 nl of AAV2-Ef1α-fDIO-mCherry into the PA. Test animals that showed correct bilateral targeting in the VMHvl and virus expression in the PA were included in the final analysis ($n = 7$ out of 9).

For optogenetic stimulation of the PA-VMHvl projection, 120 nl of AAV2-Ef1α-DIO-ChR2-eYFP was bilaterally injected into the PA of *Esr1-2A-cre* mice. Control *Esr1-2A-cre* mice received 100 nl of AAV2-CAG-FLEX-GFP bilaterally into the PA. During the same surgery, a 200-μm optic fibre assembly (Thorlabs, FT200EMT, CFLC230) was implanted 200 μm above each side of the VMHvl. Only animals with confirmed bilateral expression of ChR2–eYFP or GFP in the PA and correct bilateral fibre placements in the VMHvl were included in the final analysis (ChR2–eYFP: $n = 14$ out of 17; GFP: $n = 11$ out of 11).

For optogenetic stimulation of $VMHvl^{Npy2r}$ cells, 120 nl of AAV2-Ef1α-DIO-ChR2-eYFP was bilaterally injected into the VMHvl of *Npy2r-ires-cre* mice. During the same surgery, a 200-μm optic fibre assembly (Thorlabs, FT200EMT, CFLC230) was implanted 200 μm above each side of the VMHvl. Only animals with confirmed bilateral expression of ChR2–eYFP and correct fibre placements were included in the final analysis (ChR2–eYFP: $n = 3$ out of 3).

For optogenetic stimulation of PVN^{Oxt} cells, 120 nl of AAV2-Ef1α-DIO-ChR2-eYFP was bilaterally injected into the PVN of *Oxt-ires-cre* mice (bregma coordinates: AP, −0.80 mm; ML, ±0.250 mm; DV, −4.50 mm). Control *Oxt-ires-cre* mice received 100 nl of AAV2-CAG-FLEX-GFP bilaterally into the PVN. During the same surgery, a 200-μm optic fibre assembly (Thorlabs, FT200EMT, CFLC230) was implanted 200 μm above each side of the PVN. Only mice with confirmed bilateral expression of ChR2–eYFP or GFP and correct fibre placements were included in the final analysis (ChR2–eYFP: $n = 5$ out of 6; GFP: $n = 6$ out of 6).

For combined pharmacological inhibition of PA OXTR and optogenetic stimulation of PVN^{Oxt} cells, 120 nl of AAV2-Ef1α-DIO-ChR2-eYFP was bilaterally injected into the PVN. During the same surgery, a 200-μm optic fibre assembly (Thorlabs, FT200EMT, CFLC230) was implanted 200 μm above the PVN, and cannulae (RWD Life Science, 62102) were implanted 500 μm above the PA bilaterally. Only animals with confirmed bilateral expression of ChR2–eYFP in the PVN and correct placements of both fibre and cannulae were included in the final analysis ($n = 7$ out of 7).

For fibre photometric recording of $PA^{Esr1 \rightarrow VMHvl}$ cells, 130 nl of HSV-hEf1α-LS1L-Flpo was injected into the VMHvl, and 120 nl of AAV8-Ef1α-fDIO-GCaMP6s was injected into the ipsilateral PA of *Esr1-2A-cre* mice. A custom-made optic-fibre assembly (Thorlabs, FR400URT, CF440) was then implanted around 150 μm above the dorsal boundary of the PA and secured with dental cement (C&B Metabond, S380). Recordings commenced 3 weeks after virus injection, during both virgin and lactating states. Only animals with confirmed unilateral VMHvl targeting, correct GCaMP6s expression and proper fibre placement in the PA were included in the final analysis ($n = 16$ out of 19).

For fibre photometric recording of $VMHvl^{Npy2r}$ cells, 120 nl of AAV2-CAG-FLEX-GCaMP6f-WPRE-SV40 was injected into the VMHvl of

Npy2r-ires-cre mice. A custom-made optic fibre assembly (Thorlabs, FR400URT, CF440) was then implanted ~150 µm above the dorsal boundary of the VMHvl and secured with dental cement (C&B Metabond, S380). Recordings began 3 weeks after virus injection. Only animals with confirmed GCaMP6f expression in the VMHvl were included in the final analysis ($n = 6$ out of 7).

For combined fibre photometry recording of VMHvl-projecting PA cells and optogenetic stimulation of PVN^{Oxt} cells, 130 nl of AAVrg-Ef1α-Flpo was injected into the VMHvl, 120 nl of AAV8-Ef1α-fDIO-GCaMP6s into the ipsilateral PA and 120 nl of AAV2-Syn-FLEX-ChrimsonR-tdTomato was bilaterally injected into the PVN of *Oxt-ires-cre* mice. During the same surgery, a 400-µm optic fibre assembly (Thorlabs, FR400URT, CF440) was implanted unilaterally, around 200 µm above both the PVN and PA. Only animals with confirmed bilateral ChrimsonR-tdTomato expression in the PVN, GCaMP6 expression in the PA and correct fibre placements were included in the final analysis ($n = 6$ out of 8).

For pharmacological inhibition of OXTR, cannulae (RWD Life Science, 62102, 62129) were bilaterally implanted 0.5 mm above the PA or VMHvl of WT mice. Animals included in the final analysis were as follows: PA, 10 out of 11 (C57 × SW F_1 hybrid); PA, 3 out of 3 (SW); VMHvl, 7 out of 7 (C57 × SW F_1 hybrid).

For conditional *Oxtr* knockout, 200 nl of AAV1-CMV-HI-eGFP-cre was bilaterally injected into the PA or VMHvl. Control animals received 100 nl of AAV2-hSyn-GFP bilaterally in the same regions. Only animals with confirmed GFP expression in the PA or VMHvl were included in the final analysis (PA with *eGFP-cre*: $n = 8$ out of 9; PA with GFP: $n = 7$ out of 7; VMHvl with *eGFP-cre*: $n = 6$ out of 6; VMHvl with GFP: $n = 5$ out of 5).

For slice recordings of VMHvl-projecting PA^{Esr1} cells, 30 red retrobeads (Lumafluor, R170) were bilaterally injected into the VMHvl of *Esr1-zsGreen* mice. Brains were collected for recording 7–10 days later, with females in either the virgin or lactating state. Only animals with confirmed VMHvl targeting were included in the final analysis ($n = 4$ out of 4).

For slice recordings of $VMHvl^{Npy2r}$ cells, 100 nl of AAV2-CAG-FLEX-GFP was bilaterally injected into the VMHvl of *Npy2r-ires-cre* mice. Brains were collected for recording 3–4 weeks later, with females in either the virgin or lactating state. Only animals with confirmed VMHvl targeting were included in the final analysis ($n = 15$ out of 15).

To probe responses of $VMHvl^{Npy2r}$ and $VMHvl^{Npy2r(-)Esr1(+)}$ cells to PA inputs, 200 nl of AAV5-hSyn-Chronos-GFP was bilaterally injected into the PA, and 200 nl of a 1:1 mixture of AAV2-CAG-FLEX-GFP and AAV8-Ef1α-Coff/Fon-mCherry was bilaterally injected into the VMHvl of *Npy2r-ires-cre* × *Esr1-2A-Flpo* mice. Brains were collected for recording 3–4 weeks later, with females in either the virgin or lactating state. Only animals with confirmed VMHvl targeting were included in the final analysis ($n = 14$ out of 14).

To examine the effect of oxytocin on PA^{Esr1} cells, 120 nl of AAV2-Ef1α-fDIO-mCherry was bilaterally injected into the PA of *Esr1-2A-Flpo* mice. Brains were collected for recording 3–4 weeks later, with females in either the virgin or lactating state. Only animals with confirmed PA targeting were included in the final analysis ($n = 4$ out of 4).

Behavioural analysis

Animal behaviours in all experiments were video recorded from both the side and top of the cage using two synchronized cameras (Basler, acA640-100gm) and commercial acquisition software (StreamPix 5, Norpix) in a semi-dark room with infrared illumination at 25 fps. Behavioural annotation and tracking were performed frame by frame using custom MATLAB software (https://pdollar.github.io/toolbox/). For female sexual behaviours, definitions were as follows: lordosis—the female was on the ground, motionless or arched her back while the male was mounting or intromitting. The lordosis quotient was calculated as the ratio of lordosis events to male mounting events. The deep-thrust success rate was calculated as the ratio of mounts followed by intromission to total mount events. For male sexual behaviours: shallow thrust—the male placed his forelegs over the female's back with hindlimbs on the ground, accompanied by shallow pelvic thrusts; deep thrust—a deep, rhythmic thrust following the shallow thrust. For aggression: attack was defined as a sequence of actions initiated by the resident toward the juvenile intruder, including lunges, bites, tumbling and rapid locomotion between such behaviours. Investigation was defined as nose contact with any part of the stimulus animal. Pup retrieval was defined as lifting a pup with the jaw until it was placed in or near the nest. All mouse behaviours were manually annotated frame by frame by experimenters who were either blinded or not blinded to group assignment. We compared annotations of 15 videos performed both blinded and non-blinded and found a high level of consistency.

Female aggression test

To assess female aggression, we performed the resident–intruder (RI) test during the dark cycle (22:00 to 04:00). A male or female juvenile intruder (19–28 days old), an adult C57BL/6N male or an adult C57BL/6N female was introduced into the female's home cage (Sealsafe Plus, GM500, 39.1 × 19.9 × 16 cm) for 10 min. No differences were observed in female aggression toward male versus female juvenile intruders.

To evaluate aggression across reproductive states, RI tests were conducted at approximately the same time the day before mating and on postpartum days 1, 3, 5, 7, 14 and 21. When multiple intruders were tested on the same day, the juvenile intruder was always tested first, followed by adult female and adult male intruders, with at least a 2 min interval between tests. During the postpartum period, pups were removed 15 min before the RI test and returned immediately afterward.

To examine the effect of pup separation on maternal aggression, all pups were removed from the home cage of lactating females on postpartum day 3 and cared for by a foster female. Then, 24 h after pup removal, a juvenile mouse was introduced into the test female's cage for 10 min. After behavioural testing, the pups were returned to the mother's cage, and maternal aggression towards a juvenile intruder was reassessed 24 h later.

Fibre photometry

Due to loss of Ca^{2+} signals in the PA after prolonged virus incubation in some animals, GCaMP6 activity of $PA^{Esr1→VMHvl}$ cells was recorded during virgin and lactating states in separate groups of females. For virgin females, recordings began 3–4 weeks after virus injection. Oestrous and dioestrous states were determined through vaginal cytology, and females were recorded during dioestrus and oestrus on separate days. During each recording session, a male or female juvenile (19–28 days old) was introduced into the cage for 10 min. For lactating females, animals were co-housed with males 3–4 days after surgery until pregnancy was visually confirmed. Cages were checked daily, and the day that pups were first observed was designated PPD1. Recordings in the lactating state were conducted on PPD3–PPD5, typically 4–5 weeks after virus injection. During these sessions, pups were temporarily removed, and a male or female juvenile (19–28 days old) was introduced for 10 min.

For head-fixed recording, mice were habituated to head fixation for at least 3 days, 30 min per day. On the recording day, mice were head-fixed immediately after the RI test. An anaesthetized male, female or juvenile C57BL/6N mouse, or a 15 ml conical tube, was placed approximately 2 mm in front of the recording mouse's nostrils by an experimenter. Each stimulus was presented four times for 5 s, with 20 s intervals between presentations and 1 min between different stimuli.

For fibre photometry recording of $VMHvl^{Npy2r}$ cells, Ca^{2+} activity was monitored in the same females during both virgin and lactating states. Then, 3 weeks after virus injection, recordings were performed during dioestrus and oestrus. During each session, a male or female juvenile (19–28 days old) was introduced for 10 min. Subsequently, each female was paired with an adult male, and the male was removed once

the female became visibly pregnant. Cell responses to a juvenile intruder were then recorded for 10 min on PPD3–PPD5.

The fibre photometry setup was as previously described[11,16]. In brief, a 390 Hz sinusoidal blue LED light (30 µW; LED, M470F1; LED driver, LEDD1B; Thorlabs) was band-pass filtered (passing band: 472 ± 15 nm; FF02-472/30-25, Semrock) and delivered to the brain to excite GCaMP6. Emission light travelled back through the same optic fibre, was band-pass filtered (passing band: 535 ± 25 nm; FF01-535/505, Semrock), passed through an adjustable zoom lens (SM1NR01, Thorlabs; Edmund Optics, 62-561), detected by a Femtowatt Silicon Photoreceiver (Newport, 2151) and recorded using a real-time processor (RZ5, TDT). The envelope of the 390 Hz signals, reflecting GCaMP6 intensity, was extracted in real time using a custom TDT OpenEx program and low-pass filtered at 5 Hz. For data analysis, the MATLAB function msbackadj with a moving window of 25% of the total recording duration was first applied to obtain the instantaneous baseline signal. The instantaneous $\Delta F/F$ was calculated as: $\Delta F/F = (F_{raw} - F_{baseline})/F_{baseline}$. Peri-event time histograms were constructed by aligning $\Delta F/F$ signals to behaviour onset. The peak $\Delta F/F$ for each behavioural episode was defined as the maximum $\Delta F/F$ from 0 to 3 s after behaviour onset minus the average $\Delta F/F$ from −10 to −1 s before onset. The introduction peak $\Delta F/F$ for each stimulus was calculated as the maximum $\Delta F/F$ from 0 to 10 s after stimulus introduction minus the average $\Delta F/F$ from −15 to −1 s before onset.

Pharmacogenetic inactivation

To examine the effect of PA^{Esr1} or $PA^{Esr1\rightarrow VMHvl}$ inhibition on female sexual behaviours, the oestrous state of each female was first determined through vaginal cytology on the test day. If a female was in oestrus, a highly sexually experienced male was introduced into her home cage for around 5 min to assess sexual receptivity. The male typically attempted to mount immediately, and, if intromission occurred during this pretest, the female was considered sexually receptive and proceeded to the test.

Females first received an i.p. injection of saline. Then, 30 min later, a different sexually experienced male was introduced into the female's home cage for 10 min or until the male attempted 10 mounts. Next, 1 h later, the same female was i.p. injected with 5 mg per kg CNO (Sigma-Aldrich, C0832) and, 30 min later, a different sexually experienced male was introduced again to reassess sexual receptivity. Different males were used for each test to prevent the confounding effect of heightened sexual eagerness after previous encounters.

After the mating tests, all females were paired with males until pregnancy was visually confirmed. Maternal care and aggression were then tested during PPD3–PPD5. For the maternal care test, all pups except for one were removed immediately after CNO or saline injection. Then, 30 min later, five pups were introduced far from the nest, and interactions were observed for 10 min. Next, all of the pups were removed, and 2 min later, a male or female juvenile intruder (19–28 days old) was introduced for a 10-minute RI test. Maternal care and aggression tests were repeated the next day using the same female mice 30 min after CNO or saline injection. CNO and saline administration was counterbalanced across animals.

Optogenetic activation

After 3 weeks of viral incubation, on test days, two 200-µm or 400-µm multimode optical fibres (Thorlabs, FT200EMT, FR400URT) were connected to the bilaterally or unilaterally implanted fibre assemblies using matching sleeves (Thorlabs, ADAL1). To activate the $PA^{Esr1\rightarrow VMHvl}$ projection in virgin females, vaginal smears were examined 30 min before testing to identify dioestrous females. During the test, each female was introduced into the home cage of a sexually experienced male. After introduction, the male typically attempted to mount immediately. Once mounting occurred frequently and regularly, light pulses (5 mW, 20 Hz, 20 ms, 60 s on/60 s off) were delivered through the bilaterally implanted fibres using a laser (Shanghai Dream Laser) controlled by OpenEx (TDT). Light stimulation was repeated 5–6 times per session.

For activating PA^{Esr1} to VMHvl terminals, a male or female juvenile intruder (15–28 days old) was introduced into the female's home cage, and light pulses (5 mW or 0 mW, 20 Hz, 20 ms, 60 s on/60 s off, 5–6 times each) were delivered 2 min after intruder introduction. For activating $VMHvl^{Npy2r}$ cells in virgin females, 5 mW or 0 mW, 473 nm, 20 ms, 20 Hz light was delivered for 30 s, each for 4–5 times, 2–3 min after juvenile introduction. The order of sham (0 mW) and real (5 mW) stimulation was counterbalanced across animals. The light intensity at the fibre tip was measured during pulsing using an optical power meter (Thorlabs, PM100D).

To examine the effect of PVN^{Oxt} cell activation on the serum oxytocin levels, PA cell activity and maternal aggression, baseline aggression was first assessed 24 h after pup separation. A male or female juvenile intruder (19–28 days old) was introduced into the test female's home cage for 10 min. Subsequently, blue or yellow light (5 mW, 20 Hz, 20 ms pulses, 20 s on/40 s off) was delivered through the implanted optic fibres for 1 h. Immediately after light stimulation, a different juvenile intruder was introduced into the female mouse's cage for 10 min, during which maternal behaviours and, in some cases, PA cell responses, were monitored.

Oxtr region-specific knockout

To knock out *Oxtr* in the PA and VMHvl, we bilaterally injected 120 nl of AAV1 expressing *GFP-cre* (control: GFP) into the PA or VMHvl of $Oxtr^{flox/flox}$ female mice. We have previously shown that this approach effectively knocks out *Oxtr* in the VMHvl (ref. 46). Then, 3–5 days after surgery, each female was co-housed with a male until pregnancy was visually confirmed. Between PPD3 and PPD5, maternal aggression was assessed by introducing a juvenile intruder into the female's home cage for 10 min.

In vivo OXTR antagonist application

To block OXTR in the PA and VMHvl, cannulae (RWD Life Science, 62102, 62129) were bilaterally implanted 0.5 mm above the PA or VMHvl of female mice. Then, 3–5 days after surgery, each female was co-housed with a male until pregnancy was visually confirmed. Between PPD3 and PPD5, 100 nl of 100 µM L-371,257 hydrochloride (Tocris, 2641) was injected into each side of the PA or VMHvl through the cannula using a Hamilton syringe (65457-02) while the test animal was head-fixed on a running wheel. After injection, females were returned to their home cage. Then, 30 min later, a juvenile intruder was introduced, and the female's behaviour was observed for 10 min. Control animals received saline injections and underwent the same behavioural testing.

Measure oxytocin

Oxytocin levels in mouse tail blood were measured using a previously described method[50]. Mice were anaesthetized with 1.5% isoflurane and placed in a stereotaxic apparatus. Tail blood was collected and centrifuged at 4 °C, 1,500 rcf for 10 min to isolate serum, which was stored at −80 °C until all samples were collected. Serum oxytocin levels were then measured using an ELISA kit (Arbor Assays, K048-H5) according to the manufacturer's instructions. Blood samples were collected only once per animal to avoid repeated sampling-induced alterations in maternal behaviour or oxytocin levels.

In vitro electrophysiological recording

To prepare brain slices for patch-clamp recording, mice were anaesthetized with isoflurane, and brains were quickly removed and then immersed in ice-cold cutting solution for 1–2 min (110 mM choline chloride, 25 mM $NaHCO_3$, 2.5 mM KCl, 7 mM $MgCl_2$, 0.5 mM $CaCl_2$, 1.25 mM NaH_2PO_4, 25 mM glucose, 11.6 mM ascorbic acid and 3.1 mM pyruvic acid). PA or VMHvl coronal sections (275 µm) were cut using the Leica VT1200s vibratome, collected in oxygenated (95% O_2 and 5% CO_2) and preheated (32–34 °C) ACSF solution (125 mM NaCl, 2.5 mM KCl, 1.25 mM NaH_2PO_4, 25 mM $NaHCO_3$, 1 mM $MgCl_2$, 2 mM $CaCl_2$ and 11 mM glucose) and incubated for 30 min. The sections were then transferred to room temperature and continuously oxygenated until use.

Current and voltage whole-cell patch-clamp recordings were performed using micropipettes filled with intracellular solution containing 145 mM potassium gluconate, 2 mM $MgCl_2$, 2 mM Na_2ATP, 10 mM HEPES, 0.2 mM EGTA (286 mOsm, pH 7.2) or 135 mM $CsMeSO_3$, 10 mM HEPES, 1 mM EGTA, 3.3 mM QX-314 (chloride salt), 4 mM Mg-ATP, 0.3 mM Na-GTP and 8 mM sodium phosphocreatine (pH 7.3 adjusted with CsOH). The signals were recorded using the MultiClamp 700B amplifier (Molecular Devices) and Clampex 11.0 software (Axon Instruments), and digitized at 20 kHz with Digidata 1550B (Axon Instruments). After recording, data were analysed using Clampfit (Molecular Devices) or MATLAB (MathWorks).

To characterize the physiological and synaptic properties of PA^{Esr1}, $VMHvl^{Npy2r}$ and $VMHvl^{Npy2r(-)Esr1(+)}$ cells, we identified ZsGreen-, GFP- and mCherry-positive cells in the PA or VMHvl on slices from *Esr1-ZsGreen* mice and *Npy2r-ires-cre* × *Esr1-2A-Flpo* mice injected with floxed GFP and Coff/Fon mCherry viruses using an Olympus ×40 water-immersion objective coupled with GFP and TXRED filters. To investigate intrinsic excitability, cells were recorded in the current-clamp mode, and the number of action potentials was counted over 500-ms current steps. The current steps consisted of 18 sweeps from −20 pA to 150 pA at 10 pA per step. sEPSCs and sIPSCs were recorded in the voltage-clamp mode. The membrane voltage was held at −70 mV for sEPSC recordings and 0 mV for sIPSC recordings.

To investigate the synaptic connectivity between the PA and VMHvl, *Npy2r-ires-cre* × *Esr1-2A-Flpo* female mice were injected with 200 nl of AAV5-hSyn-Chronos-GFP into the bilateral PA and 200 nl of a 1:1 mixture of AAV2-CAG-FLEX-GFP and AAV8-Ef1α-Coff/Fon-mCherry into the bilateral VMHvl. Then, 3 weeks after virus injection and during recording, we voltage-clamp recorded *Npy2r*-expressing (GFP^+) or $Npy2r^-Esr1^+$ ($mCherry^+$) VMHvl cells and then delivered 1-ms pulses of full-field illumination using a blue LED light (pE-300white; CoolLED) at 10-s intervals to activate Chronos-expressing PA terminals. oEPSCs and oIPSCs were recorded when holding the membrane potential of recorded neurons at −70 and 0 mV, respectively (corrected for a ~6 mV liquid junction potential). oEPSPs and APs were recorded under the current-clamp mode.

To examine the effect of oxytocin on the cell properties of PA^{Esr1} cells, we injected 120 nl of AAV2-Ef1α-fDIO-mCherry into the PA of *Esr1-2A-Flpo* female mice. After 3 weeks of virus incubation, we obtained brain slices and performed current-clamp recordings of PA^{Esr1} ($mCherry^+$) cells. Cell excitability was measured by injecting 500-ms current steps before and after 250 nM TGOT perfusion. The physiological properties of the cells were characterized −10–0 min before and 10–20 min after TGOT perfusion.

Immunohistochemistry

Immunofluorescence staining was performed as previously described[16]. In brief, mice were perfused transcardially with 1× PBS followed by 4% paraformaldehyde (PFA) in 0.1 M PBS. Brains were extracted, post-fixed in 4% PFA for 3-4 h at 4 °C followed by 48 h in 20% sucrose, embedded in OCT mounting medium, frozen on dry ice, cut to 50-µm-thick sections using a cryostat (Leica Biosystems) and collected in PBS using a 12-well plate. For antibody staining, brain sections were washed with PBS three times and blocked in PBS-T (0.3% Triton X-100 in 1× PBS) with 10% normal donkey serum for 1 h at room temperature. The sections were then incubated in primary antibody diluted in blocking solution at 4 °C for 24–72 h. We stained for ESR1 (rabbit anti-ESR1; 1:1,000; Invitrogen, PA1-309, YG378288) or FOS (guinea pig anti-FOS; 1:1,000, Synaptic Systems, 226 308). The sections were then washed with PBS-T three times and incubated in secondary antibodies diluted in blocking solution (donkey anti-rabbit or guinea pig, Alexa Fluor 488 or Cy3, 1:1,000; Jackson ImmunoResearch, 711-545-152, 711-165-152 and 706-165-148) with DAPI (1:20,000, Thermo Fisher Scientific, D1306) or NeuroTrace 435/455 Blue Fluorescent Nissl Stain (1:200, Thermo Fisher Scientific, N21479) for 2–3 h at room temperature. The sections were then washed three times with PBS, mounted onto Superfrost slides (Thermo Fisher Scientific, 12-550-15), and coverslipped for imaging on a confocal microscope (Zeiss LSM 700 microscope) and/or a virtual slide scanner (Olympus, VS120).

Fluorescence in situ hybridization

Extracted brains were frozen on dry ice, and 18-µm coronal sections were prepared using a cryostat (Leica Biosystems). RNAscope labelling was performed for all genes using *Esr1* (478201-C1), *Npy2r* (315951-C2) and *Oxtr* (412171-C3) probes (Advanced Cell Diagnostics) according to the manufacturer's instructions[26].

Dual in situ hybridization and immunohistochemistry

Brain sections were treated with protease-free PretreatPro reagent according to the manufacturer's protocol. After RNA in situ hybridization, the sections were blocked in PBS-T (0.3% Triton X-100 in 1× PBS) containing 10% normal donkey serum and 1% BSA for 30 min at room temperature. The sections were then incubated with mCherry primary antibody (rabbit anti-DsRed, 1:1,000, Takara, 632496) diluted in PBS-T with 1% BSA for 1 h at room temperature. After two washes in PBS-T, sections were incubated with secondary antibodies (donkey anti-rabbit, Alexa Fluor 594, 1:500; Thermo Fisher Scientific, A21207) diluted in PBS-T with 1% BSA.

Cell counting and axon-terminal quantification

To analyse labelled cells, ×20 confocal or epifluorescence images were acquired, and cells were counted manually using ImageJ.

For DAPI-, Nissl-, CTB- and ESR1-positive cells, ×20 fluorescence confocal images were acquired. For GCaMP6- and mCherry-positive cells in pharmacogenetic and fibre photometry experiments, ×20 fluorescence images were obtained using a virtual slide scanner (Olympus, VS120). For *Esr1*-, *Npy2r*- and *Oxtr*-positive cells, ×20 fluorescence confocal images were acquired. To quantify single-cell expression of *Esr1*, *Npy2r* and *Oxtr*, puncta in ten individual cells from a single section were manually counted by a blinded experimenter using the ImageJ Cell Counter plugin.

To quantify the PA^{Esr1} axon density in the VMHvl, a 200 × 200 μm^2 boxed area containing fibres was selected in each subregion, and the average pixel intensity (F_{raw}) was measured using ImageJ and Photoshop. A same-size area in the dorsomedial VMH (VMHdm) lacking fibre terminals was used to determine background intensity ($F_{background}$). F_{signal} was then calculated as $F_{raw} - F_{background}$. For each animal, F_{signal} was normalized to the maximum F_{signal} across all analysed regions. The normalized F_{signal} values were then used to calculate the average terminal field intensity across animals.

Statistics

Sample sizes were not predetermined statistically but are comparable to previously reported studies[16,49]. All experiments were conducted using 2 to 11 cohorts of animals. For functional and in vivo recording experiments, histology images were collected from all animals. For slice recording experiments, histology images were only collected from a subset of animals, although the correct virus expression was always confirmed during the recording on the basis of the fluorescence protein expression. Histology images are representative and qualitatively similar to images from other animals. The results were reproducible across cohorts and combined for final analysis. All statistical analyses were performed using MATLAB 2020a (MathWorks) or Prism 10 (GraphPad). All datasets were tested for normality with the Shapiro–Wilk test, except for repeated-measures two-way ANOVA, mixed-effects analysis, Cochran's *Q* test, McNemar test, χ^2 test and Fisher's exact test. For datasets that passed the normality test, parametric tests were applied, including unpaired *t*-tests, paired *t*-tests, and repeated-measures or ordinary one-way ANOVA with Geisser–Greenhouse correction followed by Tukey's multiple-comparison post hoc test. For datasets that did not meet normality criteria, nonparametric tests were used,

including the Mann–Whitney *U*-test, Wilcoxon matched-pairs signed-rank test, Friedman test with Dunn's multiple-comparison post hoc test and Kruskal–Wallis test with Dunn's multiple-comparison test. Repeated-measures and ordinary two-way ANOVA with Bonferroni's multiple-comparison post hoc test were used for analyses involving two variables. Mixed-effects models were used to analyse repeated-measures data with missing values. Post hoc Bonferroni's tests were performed after repeated-measures two-way ANOVA or mixed-effects analysis. Categorical data were analysed using Cochran's *Q* test, χ^2 test, McNemar test or Fisher's exact test. When multiple pairwise comparisons were performed, *P* values were adjusted using the FDR (FDR = 0.05). Details of each statistical test, including exact *P* values, *F* values, *t* values, d.f. and cohort numbers, are provided in Supplementary Table 1. All error bars or error shades represent ±s.e.m. All *P* and *q* values equal to or smaller than 0.05 are indicated in the figures.

Reporting summary

Further information on research design is available in the Nature Portfolio Reporting Summary linked to this article.

Data availability

Behavioural annotations, fibre photometry, slice electrophysiology and raw representative histology images can be downloaded from Zenodo (https://doi.org/10.5281/zenodo.18394527)[51]. Behaviour videos and additional histology images are available from the corresponding authors on reasonable request. They have not been deposited in a public database owing to their large size and size limitation of online depositories. Source data are provided with this paper.

Code availability

MATLAB codes used in this study can be downloaded from Zenodo (https://doi.org/10.5281/zenodo.18394527)[51].

48. Fenno, L. E. et al. Comprehensive dual- and triple-feature intersectional single-vector delivery of diverse functional payloads to cells of behaving mammals. *Neuron* **107**, 836–853.e811 (2020).
49. Fang, Y. Y., Yamaguchi, T., Song, S. C., Tritsch, N. X. & Lin, D. A hypothalamic midbrain pathway essential for driving maternal behaviors. *Neuron* **98**, 192–207.e110 (2018).
50. Gnanadesikan, G. E., Hammock, E. A. D., Tecot, S. R., Carter, C. S. & MacLean, E. L. Specificity of plasma oxytocin immunoassays: a comparison of commercial assays and sample preparation techniques using oxytocin knockout and wildtype mice. *Psychoneuroendocrinology* **132**, 105368 (2021).
51. Yamaguchi, T. et al. Data and code for 'The neural mechanisms supporting the rise and fall of maternal aggression'. *Zenodo* https://doi.org/10.5281/zenodo.18394527 (2026).

Acknowledgements We thank all of the members of the Lin laboratory for discussions; Y. Jiang for assistance with genotyping; P. Dua for help with behavioural annotation and genotyping; L. Mei for generating brain atlas images; X. Yong for sharing the *Esr1-zsGreen* mouse line; S. Liberles for the *Npy2r-ires-cre* mouse; K. Deisseroth and the INTRSECT 2.0 Project for the pAAV-Ef1a-Coff/Fon-mCherry plasmid; and B. Lim for the AAV-Ef1α-fDIO-hM4Di-mCherry plasmid. This research was supported by US National Institites of Health grants R01HD116127, R01MH101377 and U19NS107616 (D.L.), R01NS049488, R01HD109519 and R01HD108363 (N.M.S.), and R35GM147119 (M.E.P.); the Brain Research Foundation (D.L.); theVulnerable Brain Project (D.L.); an Irma T. Hirschl Career Scientist Award (M.E.P); a MIND Prize from the Pershing Square Foundation (M.E.P.); the Sumitomo Foundation (T.Y.); the Research Foundation for Opto-Science and Technology (T.Y.); the Brain Science Foundation (T.Y.); the Brain and Behaviour Research Foundation (R.Y.); and a Human Frontier Science Program postdoctoral fellowship (S.P.).

Author contributions D.L. and T.Y. conceived the project, designed the experiments and wrote the paper. D.L. supervised the project. T.Y. performed all functional manipulations, in vivo recordings and histological experiments, and analysed the corresponding data. R.Y. conducted all in vitro slice recordings, analysed the data and wrote the related results. M.K. and K.T. assisted with behavioural testing and annotation. S.K. and M.E.P. contributed to histological analyses. T.O. performed preliminary experiments on the role of VMHvl OXTR in maternal aggression. S.P. and N.M.S. generated the *Esr1-2A-Flpo* knock-in mice.

Competing interests The authors declare no competing interests.

Additional information
Supplementary information The online version contains supplementary material available at https://doi.org/10.1038/s41586-026-10354-5.

Correspondence and requests for materials should be addressed to Takashi Yamaguchi or Dayu Lin.

Peer review information *Nature* thanks Oliver Bosch, Yoh Isogai and the other, anonymous, reviewer(s) for their contribution to the peer review of this work. Peer reviewer reports are available.

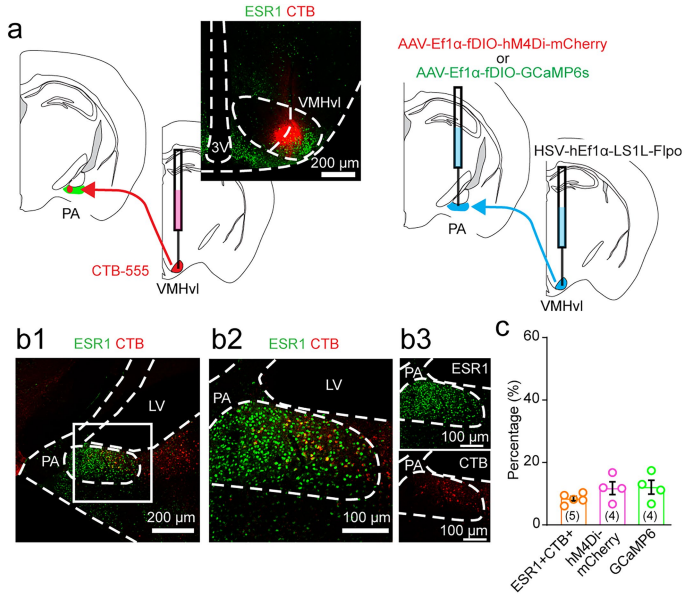

Extended Data Fig. 1 | Comparison of the retrograde labelling efficiency of HSV versus CTB. a, (Left) Experimental schematics and representative images showing Esr1 expression (green) and Alexa Fluor 555 Conjugated CTB (red) injected into the VMHvl. 3 V, third ventricle. (Right) Schematics showing the viral strategy to label PA cells projecting to the VMHvl. Brain illustrations are adapted from the Allen Brain Reference Atlas (https://atlas.brain-map.org). **b**, Representative images showing Esr1 expression (green) and CTB retrogradely labelled from the VMHvl (red) in the PA. Panels (**b2**) and (**b3**) show enlarged views of the boxed area in (**b1**). **c**, Percentage of CTB and Esr1 double-positive, hM4Di-mCherry-expressing, and GCaMP6f-expressing cells among all PA cells, based on DAPI staining. Bars and error bars represent mean ± s.e.m., and numbers in parentheses indicate the number of animals. Statistics: Ordinary one-way ANOVA followed by Tukey's multiple-comparison test. All tests are two-sided. All p values > 0.05. See Supplementary Table 1 for more detailed statistics.

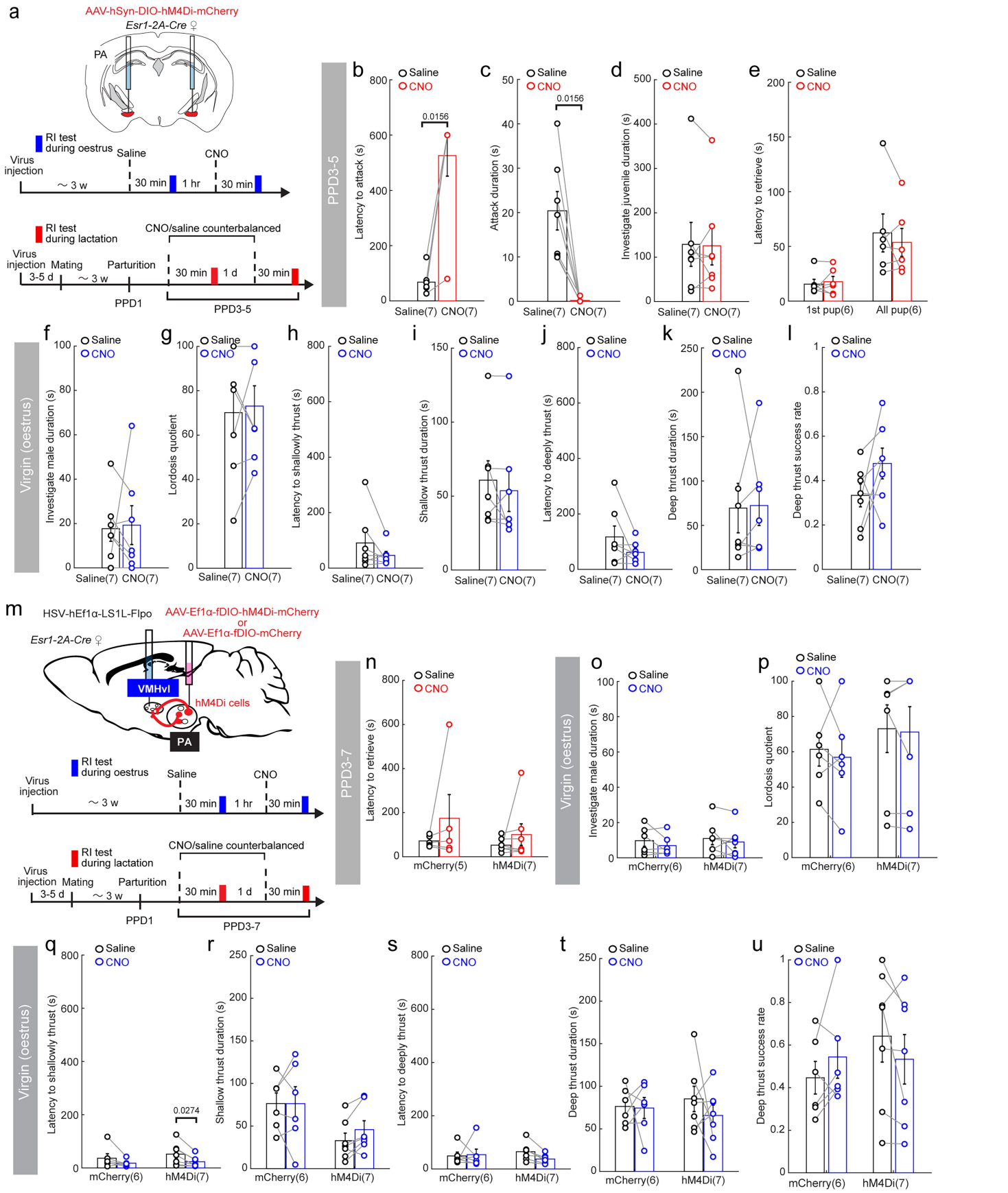

Extended Data Fig. 2 | See next page for caption.

Extended Data Fig. 2 | Chemogenetic inhibition of PA^{Esr1} and $PA^{Esr1\rightarrow VMHvl}$ cells impairs maternal aggression without affecting maternal care or sexual receptivity. a, Experimental schematic and timeline to examine behavioural changes after inhibiting PA^{Esr1} cells. Brain illustrations are adapted from the Allen Brain Reference Atlas (https://atlas.brain-map.org). **b-d**, Attack latency (**b**), attack duration (**c**), and time spent investigating juvenile intruders (**d**) after saline or CNO injections in lactating females that expressed hM4Di in PA^{Esr1} cells. **e**, The latency to retrieve the first pup and all 5 pups after saline or CNO injections in lactating females expressing hM4Di in PA^{Esr1} cells. **f, g**, Male investigation duration (**f**) and lordosis quotient (**g**) after saline or CNO injections in virgin oestrus females expressing hM4Di in PA^{Esr1} cells. **h-l**, Latency to shallow thrust (**h**), duration of shallow thrust (**i**), latency to deep thrust (**j**), duration of deep thrust (**k**), and deep thrust success rate (**l**) when sexually experienced males mated with oestrus females expressing hM4Di in PA^{Esr1} cells and receiving either CNO or saline injections. **m**, Experimental schematic or timeline to examine changes in maternal and sexual behaviours after inhibiting VMHvl projecting PA^{Esr1} cells. **n**, Latency to retrieve the first pup and all 5 pups after saline or CNO injection in lactating females expressing hM4Di in $PA^{Esr1\rightarrow VMHvl}$ cells. The latency was set to 600 s if no retrieval occurred. **o, p**, Male investigation duration (**o**) and lordosis quotient (**p**) after saline or CNO injection in virgin oestrus females expressing hM4Di in $PA^{Esr1\rightarrow VMHvl}$ cells. **q-u**, Latency to shallow thrust (**q**), shallow thrust duration (**r**), latency to deep thrust (**s**), deep thrust duration (**t**), and deep thrust success rate (**u**) when sexually experienced males mated with oestrus females expressing hM4Di in $PA^{Esr1\rightarrow VMHvl}$ cells, receiving either CNO or saline injection. All bars and error bars represent mean ± s.e.m. Numbers in parentheses indicate the number of animals. Statistical significance was determined using (**b-d,e**: 1st pup, **h, i k**) Wilcoxon matched-pairs signed-rank test, (**e:** all pup, **f, g, j, l**) paired-t-test and (**n-u**) Mixed-effects analysis with repeated measures followed by Bonferroni's multiple-comparison test. All tests are two-sided. All p values < 0.05 are indicated. See Supplementary Table 1 for more detailed statistics.

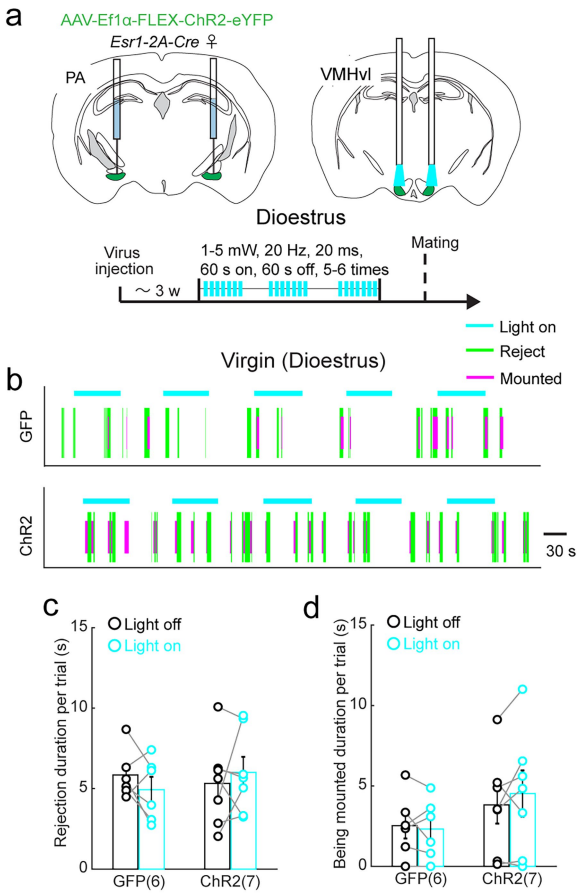

Extended Data Fig. 3 | Optogenetic activation of PA^{Esr1} to VMHvl projection does not alter female sexual receptivity. a, Experimental schematic and timeline. Brain illustrations are adapted from the Allen Brain Reference Atlas (https://atlas.brain-map.org). **b**, Representative raster plots showing behaviours of virgin dioestrus females expressing ChR2 in PA^{Esr1} cells during interaction with a male intruder when blue light was delivered to the VMHvl. Top: light-on period (cyan); bottom: behaviours. **c, d**, Time females spent rejecting the male (**c**), and duration of male mounting (**d**) during each light-on and light-off period. All bars and error bars represent mean ± s.e.m. Numbers in parentheses indicate the number of animals. Statistical significance was determined using (**c, d**) Mixed-effects analysis with repeated measures followed by Bonferroni's multiple-comparison test. All tests are two-sided. All p values < 0.05 are indicated. See Supplementary Table 1 for more detailed statistics.

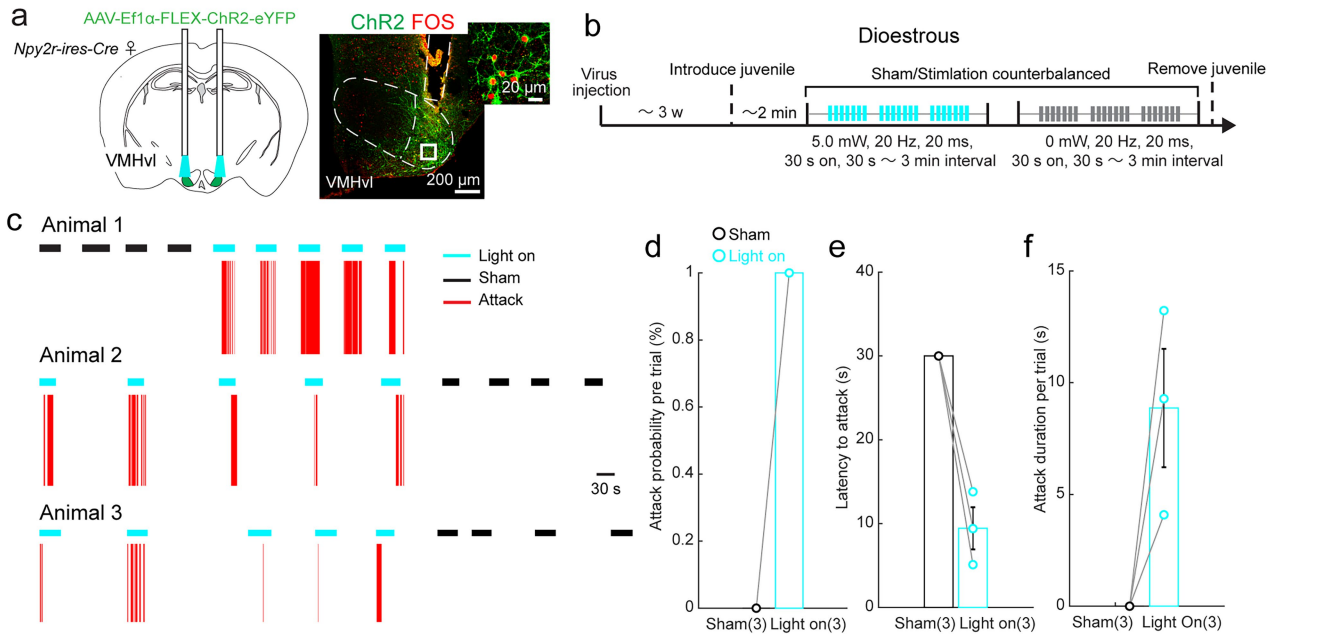

Extended Data Fig. 4 | Optogenetic activation of VMHvl^{Npy2r} cells induces time-locked attack in virgin females. a, Experimental schematic and representative images showing ChR2 (green) and Fos (red) expression in VMHvl. Right panel: enlarged view of the boxed area. Brain illustrations are adapted from the Allen Brain Reference Atlas (https://atlas.brain-map.org). **b**, Experimental timeline. **c**, Representative raster plots showing behaviours of virgin females expressing ChR2 in VMHvl^{Npy2r} cells during interaction with a juvenile intruder, with blue or sham light delivered to VMHvl. Top: sham (black) or light (cyan) delivery periods; bottom: behaviours. **d-f**, Percentage of trials in which animals attacked (**d**), attack latency per trial (**e**), and average attack duration per trial (**f**) toward juvenile intruders during light-on and sham trials. Bars and error bars represent mean ± s.e.m.; numbers in parentheses indicate the number of animals. Statistical significance was determined using Wilcoxon matched-pairs signed-rank test. All tests are two-sided. All p values < 0.05 are indicated. See Supplementary Table 1 for more detailed statistics.

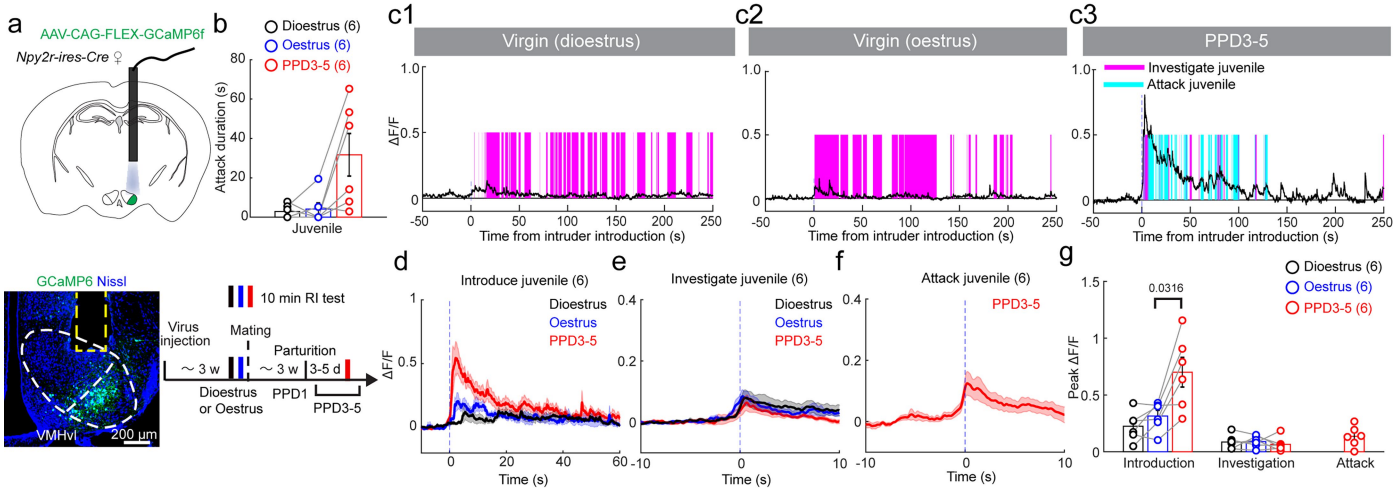

Extended Data Fig. 5 | Increased VMHvl^{Npy2r} responses to juvenile intruders in lactating females. a, Experimental schematic, test schedule, and representative image showing GCaMP6f (green) expression in VMHvl^{Npy2r} cells. Blue, Nissl. Brain illustrations are adapted from the Allen Brain Reference Atlas (https://atlas.brain-map.org). **b**, Attack duration of females toward juvenile intruders. **c**, Representative Ca^{2+} traces of VMHvl^{Npy2r} cells during interaction with a juvenile intruder in dioestrus (**c1**), oestrus (**c2**), and lactating (**c3**) females. Coloured shading indicates behavioural episodes. **d-f**, Peri-event time histograms of the Ca^{2+} signal of VMHvl^{Npy2r} cells aligned to intruder introduction (**d**), investigation (**e**) and attack onset (**f**) across dioestrus, oestrus or lactating females. **g**, Peak Ca^{2+} signal of VMHvl^{Npy2r} cells during intruder introduction, investigation, and attack. All bars and error bars and lines and shades represent mean ± s.e.m. Numbers in parentheses indicate the number of animals (**b, d-g**). Statistical significance was determined using (**b**) Friedman test with Dunn's multiple comparisons and (**g**) One-way ANOVA with repeated measures followed by Tukey's multiple-comparisons test. All tests are two-sided. All p values < 0.05 are indicated. See Supplementary Table 1 for more detailed statistics.

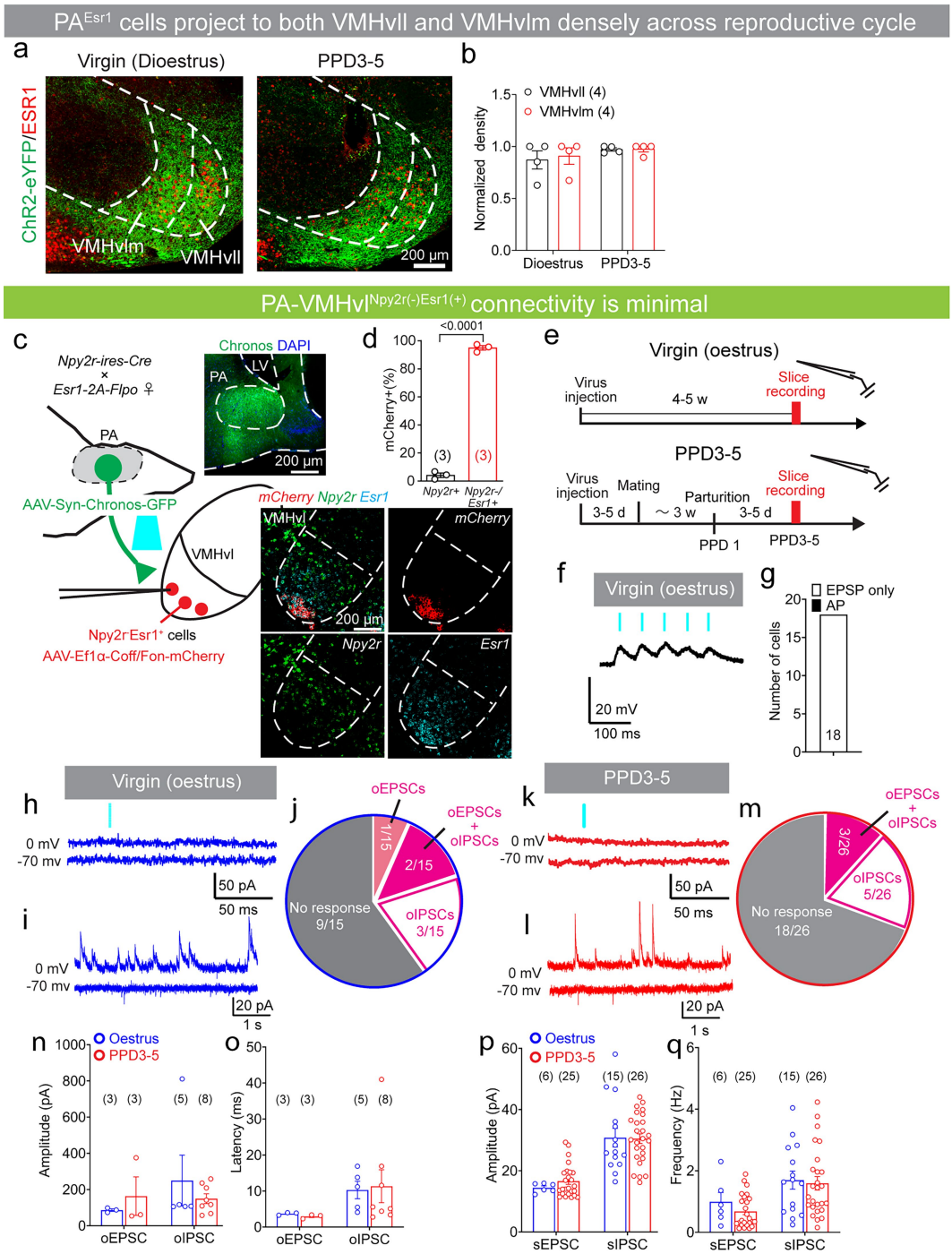

Extended Data Fig. 6 | See next page for caption.

Extended Data Fig. 6 | PA to VMHvl$^{Npy2r\text{-}Esr1+}$ cell connectivity in virgin and lactating females. a, Representative images showing terminals from PA^{Esr1} cells expressing ChR2-EYFP in the medial (VMHvlm) and lateral (VMHvll) subdivisions of the VMHvl in dioestrus and lactating females. **b**, Normalized PA^{Esr1} terminal density in VMHvlm and VMHvll of dioestrus and lactating females. F_{raw}: average pixel intensity in fibre-containing subregions; $F_{background}$: dorsal medial VMH lacking terminals; $F_{signal} = F_{raw} - F_{background}$. F_{signal} was normalized to the maximum per animal and used to calculate average terminal field density across animals. **c**, Experimental schematic for optogenetic-assisted circuit mapping. Top: Chronos-GFP expression in PA. Bottom: *mCherry* (red), *Npy2r* (green), and *Esr1* (cyan) mRNA in VMHvl and their overlap. **d**, Percentage of Npy2r+ and Npy2r-Esr1+ cells expressing mCherry. Bars and error bars represent mean ± s.e.m. Numbers in parentheses indicate the number of animals. **e**, Experimental timeline. **f**, Example voltage clamp recording trace of a VMHvl$^{Npy2r\text{-}Esr1+}$ cell in response to 5-ms blue-light pulses (blue vertical lines). **g**, The percentage of VMHvl$^{Npy2r\text{-}Esr1+}$ cells that showed PA terminal stimulation-evoked spiking in oestrus females. (n = 18 cells from 3 females). **h, i**, Example voltage-clamp recording traces of VMHvl$^{Npy2r\text{-}Esr1+}$ cells in oestrus females following 5-ms blue-light pulses (cyan) (**h**) and spontaneous activity (**i**). **j**, Pie charts showing light-evoked synaptic response patterns of VMHvl$^{Npy2r\text{-}Esr1+}$ cells in oestrus (n = 3) females. **k, l**, Example voltage-clamp recording traces of VMHvl$^{Npy2r\text{-}Esr1+}$ cells in lactating females following 5-ms blue-light pulses (cyan) (**k**) and spontaneous activity (**l**). **m**, Pie charts showing light-evoked synaptic response patterns of VMHvl$^{Npy2r\text{-}Esr1+}$ cells in lactating (n = 6) females. **n, o**, Amplitude (**n**) and latency (**o**) of oEPSCs and oIPSCs of VMHvl$^{Npy2r\text{-}Esr1+}$ cells in oestrus (n = 3) and lactating (n = 6) females. **p, q**, Amplitude (**p**) and frequency (**q**) of sEPSCs and sIPSCs of VMHvl$^{Npy2r\text{-}Esr1+}$ cells in oestrus (n = 3) and lactating (n = 6) females. Only 6/15 recorded cells in oestrus females showed sEPSC. All bars and error bars represent mean ± s.e.m. Numbers in parentheses indicate the number of subject animals (**d**) or recorded cells (**g, n-q**). Statistical significance was determined using (**b, n, o**) Mixed-effects analysis with repeated measure followed by Bonferroni's multiple-comparison test, (**d**) unpaired t-test, and (**p, q**) Mann-Whiteney test. All tests are two-sided. All p values < 0.05 are indicated. See Supplementary Table 1 for more detailed statistics.

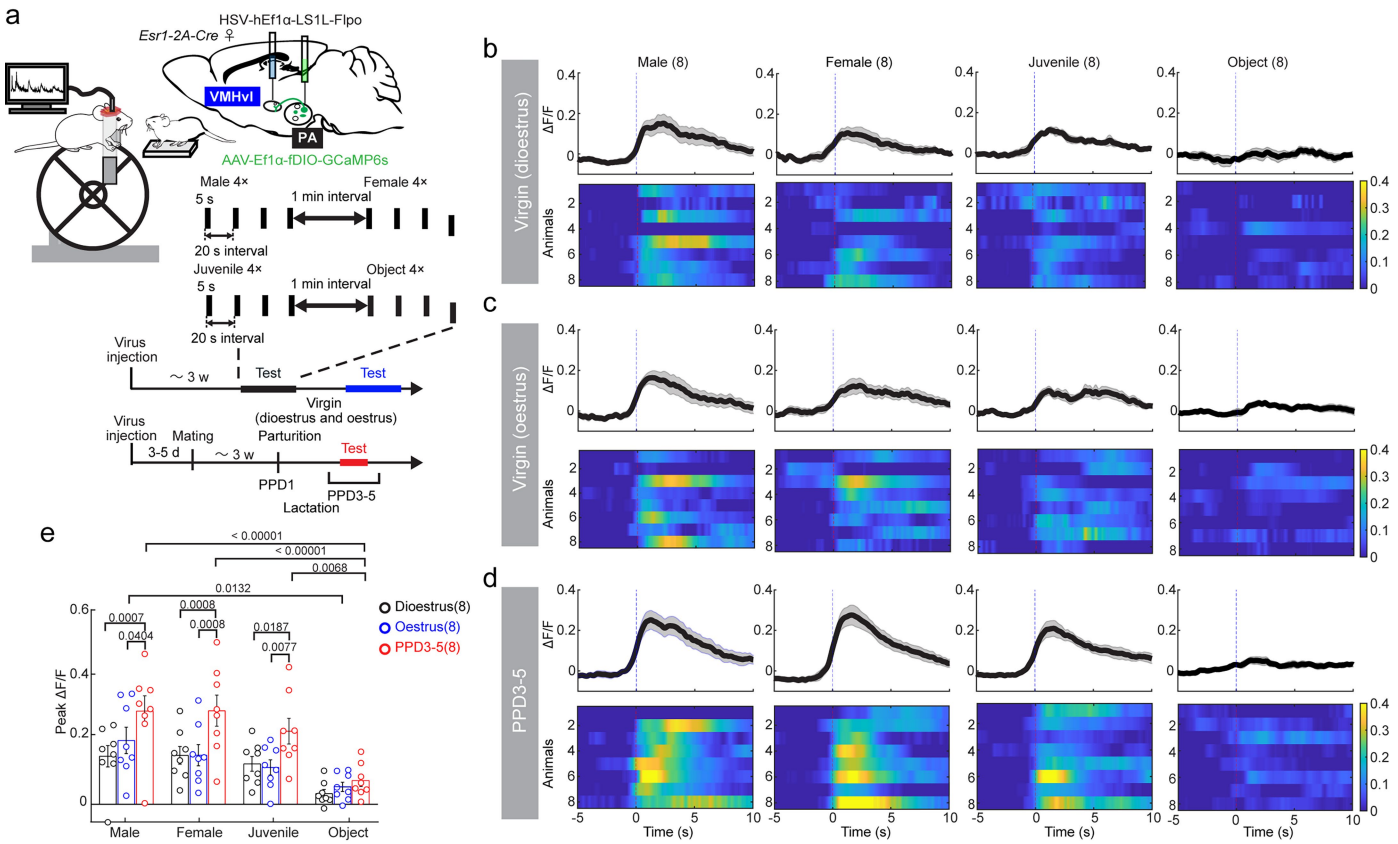

Extended Data Fig. 7 | Female PA$^{Esr1 \rightarrow VMHvl}$ cells show enhanced responses to social cues during lactation. a, Schematic of head-fixed recording setup and experimental timeline. **b-d**, Peri-event time histograms (top) and heatmaps (bottom) of PA$^{Esr1 \rightarrow VMHvl}$ cell Ca^{2+} signals aligned to the onset of adult male, adult female, juvenile, and object presentations in females during dioestrus (**b**), oestrus (**c**), and lactation (**d**). **e**, Peak ΔF/F during presentation of various stimuli in females during dioestrus, oestrus, and lactation. All data are presented as the mean ± s.e.m. Numbers in parentheses indicate the number of recording mice. Statistical significance was determined using Mixed-effects analysis with repeated-measure followed by Bonferroni's multiple-comparison test. All tests are two-sided. All p values < 0.05 are indicated. See Supplementary Table 1 for more detailed statistics.

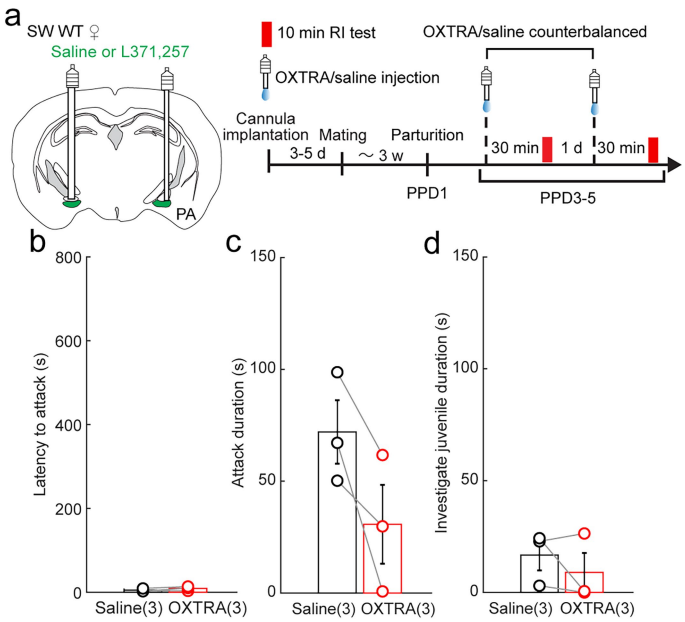

Extended Data Fig. 8 | Antagonizing OXTR in the PA impairs maternal aggression in SW females. a, Experimental schematic and timeline. Brain illustrations are adapted from the Allen Brain Reference Atlas (https://atlas.brain-map.org). **b, c, d**, Latency to attack (**b**), attack duration (**c**), and juvenile investigation duration (**d**) following injection of saline or L-371,257 hydrochloride, a potent OXTR antagonist (OXTRA), into the PA of SW females. OXTRA reduced attack duration but did not affect attack latency. All bars and error bars represent mean ± s.e.m. Numbers in parentheses indicate the number of subject animals. Statistical significance was determined using (**b**, **c**) paired t-test and (**d**) Wilcoxon matched-pairs signed rank test. All tests are two-sided. All p values < 0.05 are indicated. See Supplementary Table 1 for more detailed statistics.

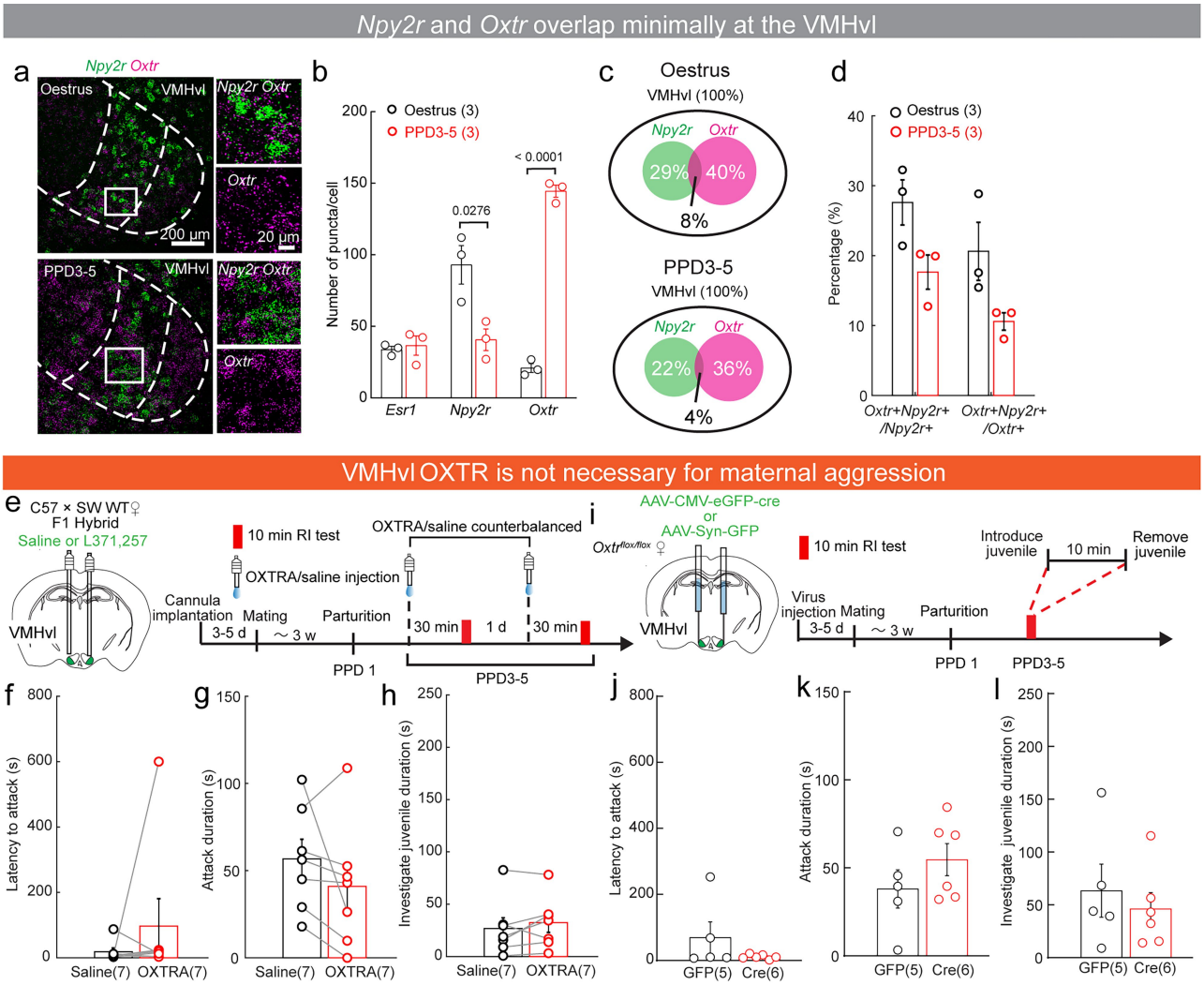

Extended Data Fig. 9 | VMHvl OXTR signalling is not essential for maternal aggression. a, Representative images showing *Oxtr* (magenta) and *Npy2r* (green) mRNA in the VMHvl of oestrus and lactating females. Right panels show enlarged views of the boxed areas. **b**, Number of *Oxtr, Npy2r* and *Esr1* mRNA puncta per corresponding Oxtr-, Npy2r- and Esr1-expressing cell in the VMHvl of oestrus and lactating females. **c**, Venn diagrams showing the percentage of *Npy2r*$^+$, *Oxtr*$^+$ and *Oxtr*$^+$*Npy2r*$^+$ cells in the VMHvl in virgin (top) and lactating (bottom) females. **d**, Percentages of *Oxtr*$^+$*Npy2r*$^+$ cells within *Npy2r*$^+$ and *Oxtr*$^+$ populations. **e**, Schematic and timeline of experiments testing the impact of VMHvl OXTR antagonism on maternal aggression. **f-h**, Attack latency (**f**), attack duration (**g**), and juvenile investigation duration (**h**) did not differ after OXTRA (red) and saline (black) injections. The attack latency was set to 600 s if no attack occurred. **i**, Schematic and timeline of experiments testing the impact of VMHvl *Oxtr* knockout on maternal aggression. **j-l**, Conditional *Oxtr* knockout in the VMHvl did not change attack latency (**j**), attack duration (**k**), and juvenile investigation duration (**l**). Bars and error bars represent mean ± s.e.m. Numbers in parentheses indicate the number of subject mice. Statistical significance was determined using (**b, d**: *Npy2r*$^+$*Oxtr*$^+$/*Npy2r*$^+$, **k**) unpaired t-test, (**d**: *Npy2r*$^+$*Oxtr*$^+$/*Oxtr*$^+$, **j, l**) Mann-Whitney test, (**f**) Wilcoxon matched-pairs signed rank test, and (**g, h**) paired t-test. All tests are two-sided. All p values < 0.05 are indicated. See Supplementary Table 1 for more detailed statistics. Brain illustrations are adapted from the Allen Brain Reference Atlas (https://atlas.brain-map.org).

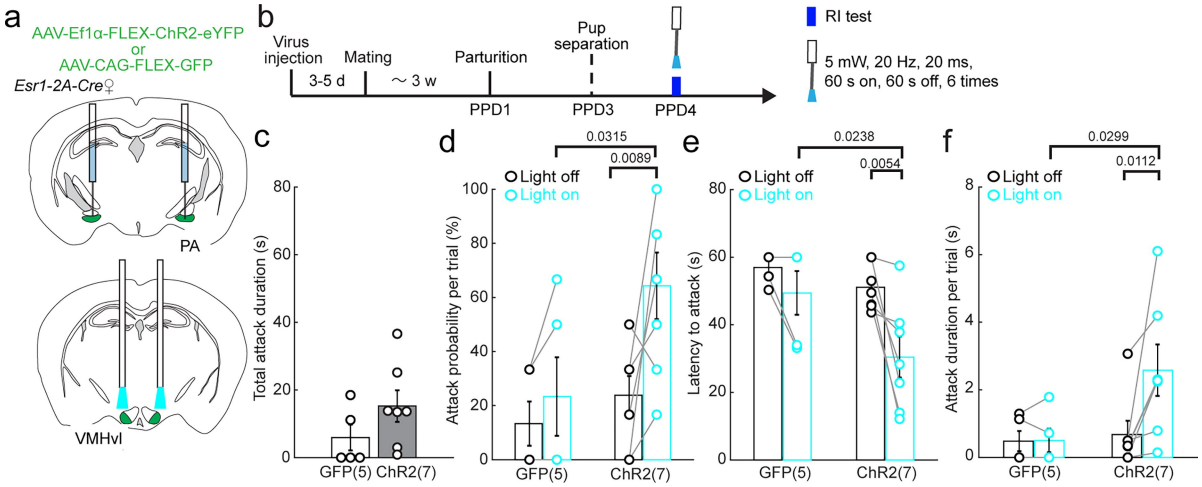

Extended Data Fig. 10 | Optogenetic activation of PA$^{Esr1\rightarrow VMHvl}$ cells is effective in promoting attack in lactating females following 24-hour pup separation. **a**, Experimental schematics. Brain illustrations are adapted from the Allen Brain Reference Atlas (https://atlas.brain-map.org). **b**, Experimental timeline used to examine the effect of PA$^{Esr1\rightarrow VMHvl}$ stimulation on maternal aggression towards juvenile intruders following pup separation. **c**, Total attack duration of ChR2 and GFP lactating females. **d**-**f**, Following 24-hour pup separation, light stimulation in lactating ChR2 animals, but not GFP animals, (**d**) increased attack probability, (**e**) decreased attack latency, (**f**) and increased the average attack duration per trial. Bars and error bars represent mean ± s.e.m. Numbers in parentheses indicate the number of animals. Statistical significance was determined using (**c**) Mann-Whitney test, and (**d**, **e**, and **f**) mixed-effects analysis with repeated-measure followed by Bonferroni's multiple-comparison test. All tests are two-sided. All p values < 0.05 are indicated. See Supplementary Table 1 for more detailed statistics.

nature portfolio

Corresponding author(s): T. Yamaguchi, D. Lin

Last updated by author(s): Jan 27, 2026

Reporting Summary

Nature Portfolio wishes to improve the reproducibility of the work that we publish. This form provides structure for consistency and transparency in reporting. For further information on Nature Portfolio policies, see our Editorial Policies and the Editorial Policy Checklist.

Statistics

For all statistical analyses, confirm that the following items are present in the figure legend, table legend, main text, or Methods section.

n/a	Confirmed	
☐	☒	The exact sample size (*n*) for each experimental group/condition, given as a discrete number and unit of measurement
☐	☒	A statement on whether measurements were taken from distinct samples or whether the same sample was measured repeatedly
☐	☒	The statistical test(s) used AND whether they are one- or two-sided *Only common tests should be described solely by name; describe more complex techniques in the Methods section.*
☒	☐	A description of all covariates tested
☐	☒	A description of any assumptions or corrections, such as tests of normality and adjustment for multiple comparisons
☐	☒	A full description of the statistical parameters including central tendency (e.g. means) or other basic estimates (e.g. regression coefficient) AND variation (e.g. standard deviation) or associated estimates of uncertainty (e.g. confidence intervals)
☐	☒	For null hypothesis testing, the test statistic (e.g. *F*, *t*, *r*) with confidence intervals, effect sizes, degrees of freedom and *P* value noted *Give P values as exact values whenever suitable.*
☒	☐	For Bayesian analysis, information on the choice of priors and Markov chain Monte Carlo settings
☒	☐	For hierarchical and complex designs, identification of the appropriate level for tests and full reporting of outcomes
☒	☐	Estimates of effect sizes (e.g. Cohen's *d*, Pearson's *r*), indicating how they were calculated

Our web collection on statistics for biologists contains articles on many of the points above.

Software and code

Policy information about availability of computer code

Data collection	Animal behaviors were recorded from both the top and side using two synchronized cameras (Basler, acA640-120um) and commercial video acquisition software (Norpix, StreamPix 5). Fiber photometry recording data was recorded using RZ5 real-time processor (Tucker-Davis Technologies). The envelope of 390-Hz 470-nm LED-induced signals from the photoreceiver were extracted in real time using a custom-written program (Tucker-Davis Technologies) as the readout of Ca2+ signal intensity. Optogenetic light stimulation was controlled using a custom-written program (Tucker-Davis Technologies). Electrophysiology data were recorded with MultiClamp 700B amplifier (Molecular Devices) and Clampex 11.0 software (Axon Instruments), digitized at 20 kHz with Digidata 1550B (Axon Instruments).
Data analysis	All statistical analysis were performed using MATLAB (R2020a), Prism (v10, Graph Pad) and ImageJ(2.11.0) software. Behaviors were analyzed manually frame-by-frame using a custom software written in MATLAB (https://pdollar.github.io/toolbox/). MATALB code used in this study can be downloaded from 10.5281/zenodo.18394527.

For manuscripts utilizing custom algorithms or software that are central to the research but not yet described in published literature, software must be made available to editors and reviewers. We strongly encourage code deposition in a community repository (e.g. GitHub). See the Nature Portfolio guidelines for submitting code & software for further information.

Data

Policy information about availability of data

All manuscripts must include a data availability statement. This statement should provide the following information, where applicable:

- Accession codes, unique identifiers, or web links for publicly available datasets
- A description of any restrictions on data availability
- For clinical datasets or third party data, please ensure that the statement adheres to our policy

Source data are provided with this paper. Behavior annotation code can be found (https://pdollar.github.io/toolbox/). Raw values associated with each figure panel can be found in the source data files. Fiber photometry recording data, behavior annotations and raw representative histology images can be downloaded from 10.5281/zenodo.18394527. Behavior videos and additional histology images are available from the corresponding author upon reasonable request.

Research involving human participants, their data, or biological material

Policy information about studies with human participants or human data. See also policy information about sex, gender (identity/presentation), and sexual orientation and race, ethnicity and racism.

Reporting on sex and gender	*Use the terms sex (biological attribute) and gender (shaped by social and cultural circumstances) carefully in order to avoid confusing both terms. Indicate if findings apply to only one sex or gender; describe whether sex and gender were considered in study design; whether sex and/or gender was determined based on self-reporting or assigned and methods used.* *Provide in the source data disaggregated sex and gender data, where this information has been collected, and if consent has been obtained for sharing of individual-level data; provide overall numbers in this Reporting Summary. Please state if this information has not been collected.* *Report sex- and gender-based analyses where performed, justify reasons for lack of sex- and gender-based analysis.*
Reporting on race, ethnicity, or other socially relevant groupings	*Please specify the socially constructed or socially relevant categorization variable(s) used in your manuscript and explain why they were used. Please note that such variables should not be used as proxies for other socially constructed/relevant variables (for example, race or ethnicity should not be used as a proxy for socioeconomic status).* *Provide clear definitions of the relevant terms used, how they were provided (by the participants/respondents, the researchers, or third parties), and the method(s) used to classify people into the different categories (e.g. self-report, census or administrative data, social media data, etc.)* *Please provide details about how you controlled for confounding variables in your analyses.*
Population characteristics	*Describe the covariate-relevant population characteristics of the human research participants (e.g. age, genotypic information, past and current diagnosis and treatment categories). If you filled out the behavioural & social sciences study design questions and have nothing to add here, write "See above."*
Recruitment	*Describe how participants were recruited. Outline any potential self-selection bias or other biases that may be present and how these are likely to impact results.*
Ethics oversight	*Identify the organization(s) that approved the study protocol.*

Note that full information on the approval of the study protocol must also be provided in the manuscript.

Field-specific reporting

Please select the one below that is the best fit for your research. If you are not sure, read the appropriate sections before making your selection.

☒ Life sciences ☐ Behavioural & social sciences ☐ Ecological, evolutionary & environmental sciences

For a reference copy of the document with all sections, see nature.com/documents/nr-reporting-summary-flat.pdf

Life sciences study design

All studies must disclose on these points even when the disclosure is negative.

Sample size	Sample sizes were not predetermined using formal statistical methods. Instead, sample sizes were chosen to reliably detect experimental effects while minimizing animal use in accordance with ethical guidelines. Sample sizes were comparable to those used in previous studies (e.g., Fang et al., 2018, Neuron; Yamaguchi et al., 2020, Nature Neuroscience) and were considered appropriate based on effect sizes, statistical significance, and consistency of results across animals.
Data exclusions	All animals included in the final analysis had correct injection sites, as verified by histology (n = 176 out of 194). For retrograde tracing experiments, only animals with confirmed targeting of the VMHvl were included in the final analysis (n = 5 of 8). For pharmacogenetic inhibition of PAEsr1 cells, test animals that showed correct bilateral targeting of the PA were included in the final analysis (n=7 out of 8).For pharmacogenetic inhibition of PAEsr1-VMHvl cells, test animals that showed correct bilateral targeting in the VMHvl and correct bilateral virus expression in the PA (n=7 out of 9) were included in the final analysis.

For the optogenetic stimulation of PA-VMHvl projection, test animals that showed correct bilateral expression of ChR2–EYFP or GFP in the PA and correct bilateral fiber placements in the VMHvl were included in the final analysis (ChR2-EYFP: n = 14 of 17; GFP: n = 11 of 11).

For the optogenetic stimulation of VMHvlNpy2r cells, test animals that showed correct bilateral expression of ChR2–EYFP and and fiber placement in the VMHvl (n = 3 out of 3) were included in the final analysis.

For the optogenetic stimulation of PVNOxy cells, test animals that showed correct bilateral expression of ChR2–EYFP or GFP and fiber placement in the PVN were included in the final analysis (ChR2–EYFP : n= 5 out of 6, GFP: n = 6 out of 6). For combined pharmacological inhibition of PA OXTR and optogenetic stimulation of PVNOxy cells, All test animals that showed correct bilateral expression of ChR2–EYFP in the PVN and correct fiber and cannulae placements in the PVN and PA were included (n=7 out of 7).

For fiber photometric recording of the PAEsr1-VMHvl cells, Animals that showed correct unilateral targeting in the VMHvl and correct expression of GCaMP6s and fiber placement in the PA were included in the final analysis (n=16 out of 19).

For fiber photometric recording of VMHvlNpy2r cells, animals that showed correct GCaMP6f expression in the VMHvl were included in the final analysis (n=6 out of 7).

For combined fiber photometric recording of VMHvl-projecting PA cells and optogenetic stimulation of PVNOXT cells, animals that showed correct GCaMP6f expression in the PA and ChrimsonR-tdTomato in the PVN were included in the final analysis (n=6 out of 8).

For pharmacological inhibition of OXTR, test animals were showed correct bilateral targeting of the PA or VMHvl were included in the final analysis. (PA, 10 of 11 (C57 × SW F1 hybrid); PA, 3 of 3 (SW); VMHvl, 7 of 7 (C57 × SW F1 hybrid)).

For the conditional gene knockout of OXTR, animals that showed GFP expression in the VMHvl or PA are included in the final analysis (PA-eGFP-Cre: n = 7 out of 9; PA-GFP m = 7 out of 7, VMH-eGFP-Cre: n = 6 out of 6; VMH-GFP: n = 5 out of 5).

For the slice recording of the VMHvl-projecting PAEsr1 cells, animals that showed correct targeting in the VMHvl were included in the final analysis (n=4 out of 4). For the slice recording of the VMHvlNpy2r cells, animals that showed correct targeting in the VMHvl were included in the final analysis (n=15 out of 15). For probing the responses of VMHvlNpy2r and VMHvlNpy2r-Esr1+ cells to PA inputs, animals that showed correct targeting in VMHvl were included in the final analysis (n=14 out of 14). For probing oxytocin effect on PAEsr1 cells, animals that showed correct targeting in PA were included in the final analysis (n=4 out of 4).

Replication

Fiber photometry recordings, immunohistochemistry, pharmacogenetic activation and inactivation, optogenetic neural activation, and in vitro electrophysiological recordings were replicated in multiple animals across independent cohorts (see statistical summaries in the Source Data tables for the exact number of animals used in each experiment).

Randomization

Mice were randomly assigned to experimental groups for comparisons such as mCherry versus hM4Di (Fig. 1c–e, Extended Data Fig. 2b–l, 2n–u), GFP versus ChR2 (Fig. 1h–q, 5g–i, Extended Data Fig. 3b–d, 10c–f), and saline versus OXTRA (Fig. 4k–m, 4o–q, 5k–l, Extended Data Fig. 9b–d, 9j–l).For histological and in vitro experiments, mice were assigned to diestrus, estrus, or lactation groups based on their reproductive state (Fig. 2b–i, 2k–t, 3l–u, 4a–c, 4e–i, 4k–m, 4o–q, 5g–i, 5s–u, Extended Data Fig. 6a,b, 6e–q).For in vivo recordings of VMHvl neurons, data were acquired longitudinally from the same animals across different reproductive states (Extended Data Fig. 5c–g). For in vivo recordings of PA neurons, mice were randomly assigned to virgin or lactating groups, including diestrus, estrus, and lactation conditions (Fig. 3d–i, 5m–r, Extended Data Fig. 7b–e).

Blinding

Experimenters were not blind to group allocation during data acquisition or analysis. However, control and experimental groups were tested under identical conditions, and all data were analyzed using the same predefined criteria. Cell counting, histological assessments, and behavioral analyses were performed independently by multiple experimenters, including both individuals who were blind and not blind to experimental conditions.

Reporting for specific materials, systems and methods

We require information from authors about some types of materials, experimental systems and methods used in many studies. Here, indicate whether each material, system or method listed is relevant to your study. If you are not sure if a list item applies to your research, read the appropriate section before selecting a response.

Materials & experimental systems

n/a	Involved in the study
☐	☒ Antibodies
☒	☐ Eukaryotic cell lines
☒	☐ Palaeontology and archaeology
☐	☒ Animals and other organisms
☒	☐ Clinical data
☒	☐ Dual use research of concern
☒	☐ Plants

Methods

n/a	Involved in the study
☒	☐ ChIP-seq
☒	☐ Flow cytometry
☒	☐ MRI-based neuroimaging

Antibodies

Antibodies used

Primary antibodies used were: rabbit anti-Esr1 antibody (1:1000, invitrogen, PA1-309), guinea pig anti-Fos antibody (1:1000, Synaptic Systems, 226 308), rabbit anti-DsRed (1:1000, Takara, 632496) . Secondary antibodies used were: Alexa 488-conjugated donkey anti-

rabbit secondary antibody (1:1000, Thermo Fisher, A11055), Alexa 594-conjugated donkey anti-rabbit (1:1000, Thermo Fisher, R37118) and Alexa 555-conjugated donkey anti-guinea pig secondary antibody (1:1000, Jackson ImmunoResearch, 706-565-148).

Validation

All the antibodies used in this paper have been used in our previous studies and cited multiple times as listed on the manufacture's website or CiteAb(https:// www.citeab.com/).
Specifically, for the primary antibodies used in this paper,
rabbit anti-Esr1 antibody (1:1000, invitrogen, PA1-309): Osakada T., et al., Nature 2024.
guinea pig anti-Fos antibody (1:1000, Synaptic System 226 308): Long, M., et al., Nature 2023.
rabbit anti-DsRed (1:1000, Takara, 632496) : Dai B., et al., Nature 2025.

Animals and other research organisms

Policy information about studies involving animals; ARRIVE guidelines recommended for reporting animal research, and Sex and Gender in Research

Laboratory animals	Mice were housed under a 12-hour light-dark cycle (dark cycle; 10 a.m. to 10 p.m. or 6:30 p.m. to 6:30 a.m.), with food and water available ad libitum. Room temperature was maintained between 20–22 °C and humidity between 30–70%, with a daily average of approximately 45%. Test animals were adult Esr1-2A-cre (>8 weeks, Jackson, 017911) mice, Npy2r-ires-cre (>8 weeks, Jackson, 029285), Esr1-Zsgreen (>8 weeks, Young Xu' lab at Baylor college), Esr1-2A-Flpo (>8 weeks, Jackson, 037009), Oxtrflox/flox (>8 weeks, Jackson, 008471) and Oxy-ires cre (>8 weeks, Jackson, 024234).Test mice were between 8 to 20 weeks at the time of behavior testing or recording. Stimulus animals in the RI tests were juvenile (3-4 weeks) and adult (>8 weeks) C57BL/6N male and female mice originally purchased from Charles River and then bred in-house. Females were considered receptive if an experienced male could mount and intromit the female within three attempts. All mice were group-housed until adulthood. After surgery, all male test mice were single-housed, while female test mice were paired with adult male mice until the females became visibly pregnant. Animals were randomly assigned to control and test groups. All experiments were performed during the dark cycle of the animals.
Wild animals	The study did not involve wild animals.
Reporting on sex	Stimulus animals in the RI tests were adult C57BL/6N (>8 weeks) male and female mice originally purchased from Charles River and then bred in-house. Only mix background female Esr1-2A-Cre, Npy2r-ires-Cre, Esr1-2A-Flpo, Oxtrflox/flox, Oxy-ires-Cre and female C57BL/6N Esr1-Zsgreen mice were used in experiments due to nature of research.
Field-collected samples	The study did not involve field collected samples
Ethics oversight	All procedures were approved by the NYULMC Institutional Animal Care and Use Committee (IACUC) in compliance with the National Institutes of Health (NIH) Guidelines for the Care and Use of Laboratory Animals.

Note that full information on the approval of the study protocol must also be provided in the manuscript.

Plants

Seed stocks	N/A
Novel plant genotypes	N/A
Authentication	N/A